M 2015

U.PORTO
FEUP FACULDADE DE ENGENHARIA
UNIVERSIDADE DO PORTO

ESTABLISHMENT AND OPTIMIZATION OF AN ALGINATE-ANCHORED TRIDIMENSIONAL IN VITRO INTESTINE MODEL FOR INTESTINAL ABSORPTION PURPOSES

SARA ISABELA BARBOSA CARNEIRO

DISSERTAÇÃO DE MESTRADO APRESENTADA
À FACULDADE DE ENGENHARIA DA UNIVERSIDADE DO PORTO EM
ENGENHARIA BIOMÉDICA

Faculdade de Engenharia da Universidade do Porto

Establishment and optimization of an alginate-anchored tridimensional in vitro intestine model for intestinal absorption purposes

Sara Isabela Barbosa Carneiro

Dissertação realizada no âmbito do
Mestrado em Engenharia Biomédica

Orientador: Bruno Sarmento, PhD
Co-Orientador: Cristina Barrias, PhD

Setembro, 2015

U.PORTO
FEUP FACULDADE DE ENGENHARIA UNIVERSIDADE DO PORTO

MEB - MESTRADO EM ENGENHARIA BIOMÉDICA | **2014/2015**

A Dissertação intitulada

"Establishment and optimization of an alginate-anchored tridimensional in vitro intestine model for intestinal absorption purposes"

foi aprovada em provas realizadas em 14-10-2015

o júri

Presidente Professor Doutor José Alberto Peixoto Machado da Silva
Professor Associado do Departamento de Engenharia Eletrotécnica e de Computadores da Faculdade de Engenharia da U. Porto

Professora Doutora Maria de La Salette de Freitas Fernandes Hipólito Reis Dias Rodrigues
Professora Associada da Faculdade de Farmácia da U. Porto

Doutor Bruno Filipe Carmelino Cardoso Sarmento
Investigador do Instituto de Engenharia Biomédica da U. Porto

O autor declara que a presente dissertação (ou relatório de projeto) é da sua exclusiva autoria e foi escrita sem qualquer apoio externo não explicitamente autorizado. Os resultados, ideias, parágrafos, ou outros extratos tomados de ou inspirados em trabalhos de outros autores, e demais referências bibliográficas usadas, são corretamente citados.

Autor - Sara Isabela Barbosa Carneiro

Faculdade de Engenharia da Universidade do Porto

Abstract

On human body, cellular growth and differentiation occus in the tridimensional environment, requiring an extracellular matrix (ECM) with which the cells interact. During the past decades, artificial 3D matrices, that mimic the natural ECM, have become increasingly relevant to overcome the gap between 2D cell culture and physiological tissue as they efficiently recreates in vivo scenarios and allow for cell-matrix interactions.

The native ECM is a hydrated gel-like substance, therefore various natural and synthetic hydrogels have been used as artificial ECM-like matrices for in vitro cell culture models. The hydrogel-based 3D microenvironments can mimic many functions of the native ECM, provide mechanical integrity to the newly formed cell-derived matrix and a hydrated space for the diffusion of nutrients and metabolites. Moreover, the ECM matrix in cell culture models enhance the natural tissue environment, biologically and physically, through the interactions between different cell types. Because cell-laden hydrogels mimic the natural tissues, they have been developed not only as a strategy for tissue repair and regeneration, but have also been used for in tissue modelling for drug development/screening and also for studying various pathological process.

This dissertation aims to develop an intestinal tissue engineering model based on intestinal fibroblasts and different epithelial cells supported by a natural biomaterial - alginate- resembling the intestinal ECM. The experimental results demonstrate that the variation of different physical and chemical parameters in the formation of alginate hydrogels allow the modulation of the properties to better recreate the mechanical characteristics found on natural intestinal scenario.

In 3D environment, we explored the behaviour of intestinal fibroblast, studying their viability, metabolic activity, morphology and ECM compounds expression, such as fibronectin and collagen. In 3D environment, these cells were characterized by a spherical shape, and the production of ECM, namely of fibronectin and collagen, was essentially restricted to the intracellular and pericellular space. The initial density of $5x10^6$ cells/mL showed to be the most suitable density to be used in the in vitro model.

Further studies consisted in characterizing the epithelium layer of intestinal mucosa through the evaluation of monolayer tightness of epithelial $C2_{BBe}1$ cells seeded on-top of the hydrogel layer, at different densities. An acceptable integrity and maturity of the monolayer was only observed for the higher density of $4x10^6$ cells/mL. Although this condition presents a

lower TEER value compared with the respective monolayer of control ($C2_{BBe}1$ 2D model), the results of permeability assays demonstrate an efficient model to predict the permeability.

Ultimately, the three-dimensional $C2_{BBe}1$ model can be the foundation for in future, development a three-dimensional co-culture model that resembles the intestinal mucosa, representing an effective tool for the early stage of drugs development.

Resumo

No corpo humano, o crescimento e a diferenciação celular ocorrem num ambiente tridimensional (3D), que requer uma matriz extracelular (ECM) com a qual as células interagem. Durante as últimas décadas, as matrizes artificiais tridimensionais, que simulam a ECM natural, tornaram-se cada vez mais relevante para superar a lacuna entre as culturas celulares bidimensionais (2D) e os tecidos fisiológicos, uma vez que as matrizes recriam de uma forma eficaz o ambiente vivo e permitem as interações célula-ECM.

A ECM nativa é uma substância semelhante a um hidrogel, por conseguinte, diferentes hidrogéis sintéticos e naturais têm sido utilizados como matrizes ECM nos modelos celulares in vitro. O microambiente 3D do hidrogel é capaz de imitar muitas funções da ECM nativa, de proporcionar uma integridade mecânica a uma matriz com células e um espaço hidratado para a difusão de nutrientes e metabolitos. Além disso, a matriz ECM nos modelos de culturas celulares melhoram o ambiente do tecido natural, biológico e físico, por meio das interações entre os diferentes tipos de células. Uma vez que os hidrogéis com células na sua matriz imitam os tecidos naturais, estes têm sido desenvolvidos não só como uma estratégia para a reparação e regeneração dos tecidos, mas também para a modelação de tecidos no desenvolvimento de fármacos/rastreio e também para o estudo de várias doenças, tais como cancro metastático.

Esta dissertação tem como objetivo desenvolver um modelo intestinal constituído por fibroblastos e diferentes células epiteliais intestinais suportados por um biomaterial natural - o alginato - que se assemelha com a ECM intestinal. Os resultados experimentais demostram que a variação de vários parâmetros físico-químicos do alginato na formação dos hidrogéis permitem a modulação das propriedades para melhor recriar as características mecânicas encontradas no cenário intestinal natural.

Num ambiente 3D, foi avaliado o comportamento dos fibroblastos intestinais, segundo a sua viabilidade, atividade metabólica, morfologia e expressão de componentes da ECM, tais como a fibronectina e o colagénio. Num ambiente 3D, os fibroblastos demostraram uma forma esférica e uma produção de fibronectina e colagénio essencialmente no espaço intracelular e pericelular. A densidade inicial de $5x10^6$ células/mL mostrou ser a densidade mais adequada para ser usada no modelo intestinal in vitro.

Outros estudos consistiram na caracterização da camada epitelial da mucosa intestinal através da avaliação da coesão da monocamada das células epiteliais $C2_{BBe}1$ sob a superfície superior da camada de hidrogel, a diferentes densidades.

Uma integridade e maturidade aceitável da monocamada foram observadas somente para a maior densidade de $4x10^6$ células/mL. Embora esta condição apresente um valor de TEER menor comparado com a respetiva monocamada de controlo (modelo $C2_{BBe}1$ 2D), os resultados dos ensaios de permeabilidade demonstram um modelo eficiente na previsão da permeabilidade.

Para finalizar, o modelo tridimensional $C2_{BBe}1$ pode ser a base para desenvolver futuramente o modelo co-cultura tridimensional que assemelha-se à mucosa intestinal, representando uma ferramenta eficaz para a fase inicial do desenvolvimento de fármacos.

Acknowledgements

This thesis was a deep and long journey in which will surely enriching myself as a person as an engineer and researcher.

I am truly grateful to my supervisor Dr. Bruno Sarmento and my co-supervisor Dra. Cristina Barrias. In all this year of research and writing of this thesis, the continuous support of my supervisors, their patience, motivation, enthusiasm and immense knowledge was extreme important.

Further, I would like to thank all the people of my group who accompanied me, helped whenever necessary and had all the patience with me.

For last, but not least, I would like thank all my friends and family for being support and strength that I needed to reach this far in my life.

" *Lute com determinação, abrace a vida com paixão, perca com classe e vença com ousadia. Porque o mundo pertence a quem se atreve e a vida é muito para ser insignificante.*" (Charles Chaplin)

Contents

List of Figures

List of Tables

Acronyms and Symbols

ACRONYMS

2D	Two-dimensional
3D	Tridimensional
ALP	Alkaline phosphatase
BB	Brush border
bFGF	Basic fibroblast growth factor
CA	Chitosan-alginate
C-PEG	Chitosan-poly (ethylene glycol)
DMEM	Dulbecco's Modified Eagle Medium
ECM	Extracellular matrix
EDC	1-ethyl-(dimethylaminopropyl)-carbodiimide
EDTA	Ethylenediamine tetraacetic acid
EGF	Epidermal growth factor
FAE	Follicle-associated epithelium
FBS	Fetal bovine serum
FN	Fibronectin
G	Guluronic acid
GDL	Glucone-δ-lactone
GI	Gastrointestinal
GPC	Gel permeation chromatography
HaCaT	Keratinocytes cells
HBSS	Hank's balanced salt solution
HepaRG	Liver progenitor cell line
hFF	Fibroblasts cells
HMW-G	High molecular weight G-rich
HMW-M	High molecular weight M-rich
HG	Hyaluronan-gelatin
H&E	Hematoxylin and eosin
IMFs	Intestinal myofibroblasts
ISCs	Intestinal stem cells
LMW-G	Low molecular weight G-rich
LMW-M	Low molecular weight M-rich
LVR	Linear viscoelastic region

M	Mannuronic acid
MALT	Mucosa-associated epithelium
MMW-G	Medium molecular weight G-rich
MMW-M	Medium molecular weight M-rich
NEAA	Non-essential aminoacids
NFC	Nanofibrillar cellulose
NPCs	Non parenchymal cells
PEG	Polyethylene glycol
PI	Propidium iodide
RFU	Relative fluorescence units
RGD	Arginine-glycine-aspartate
RT	Room temperature
Sulfo-NHS	N-Hydroxy-sulfosuccinimide
SKPs	Skin-derived precursors
TEER	Transepithelial electrical resistance
TJs	Tight junctions
Tris	Tris(hydroxymethyl)aminomethane

SYMBOLS

ΔQ	Amount of compound in basolateral side
l	Carbon-carbon
C_n	Characteristic ratio
C_p	Concentration of alginate solution
P_p	Density of alginate
P_M	Density of culture medium
C_{eff}	Effective alginate concentration
R	Gas constant
C_o	Initial concentration
G"	Loss (Viscous) modulus
ξ	Mesh size
M_n	Molecular weight
M_C	Molecular weight of between crosslinks
M_R	Molecular weight of monomer
M_{RGD}	Molecular weight of RGD
C_{nom}	Nominal alginate concentration
δ	Phase Angle
G'	Storage (Elastic) modulus
A	Surface area
q_F	Swelling ratio
T	Temperature
Δt	Time

v_2	Volume fraction
w/v	Weight/volume
w/w	Weight/weight

Chapter 1 - Introduction

1.1. Motivation and objectives

Many of the intestinal processes are difficult to analyses using only in vivo intestinal models, especially in what concerns the behavior of epithelial cells in response to specific environmental stimulus. Synthetic in vitro intestinal models can allow improved studies of intestinal functions, meeting the requirements of the 3R's policy, especially for drug absorption studies, since one of the most important factors defining the absorption of oral drug is the drug permeability across the intestinal membrane [1].

Thus, the cell culture models are becoming increasingly routine part of development of the drug pipeline in the pharmaceutical industry. This strategy has proven to be efficient and could be developed and used in the initial stages of research on oral drug delivery, reducing this way the expense and ethical issues raised by using excessive numbers of animals. Hence it is important to invest in improving existing cell models for drug absorption studies [2,3].

The Caco-2 cells has been the most frequently used model to evaluate the intestinal permeability of drugs. However, this model still has limited potentialities, since it does not cover the complexity of interactions between epithelial cells and the underlying lamina propria cells [4]. Therefore, in order to improve the Caco-2 cell-based model, co-culture cell models, which comprises different cell types present in the intestinal epithelium, have been proposed to represent the heterogeneity of the intestinal epithelium at a cellular level [4].

Our group has recently proposed a new in vitro model, based on Caco-2, mucus-producing HT29-MTX and the Raji B cells that protagonize the conversion of Caco-2 in M-like cells through soluble factors. This triple co-culture cell model can be a reliable alternative to existing models, as it provides a more physiological, functional, and reproducible in vitro model of the intestinal barrier and is therefore preferable in permeability studies [4].

Another aspect of existing cell models is the ability to be formed on 2D substrates, including Transwell® inserts. However, it is widely understood that a 3D physical environment plays a critical role in the metabolism, biochemistry and morphology of mammalian cells and thus epithelial cells cultured in 3D environments exhibit different phenotypes that are more reflective of native tissue [1]. Various natural and synthetic biomaterials have been considered as cell supporting matrices to develop 3D structure that can effectively replicate ECM. Polymers

of natural origin such alginate are attractive options, mainly due to their similarities with extracellular matrix (ECM) as well as their chemical versatility and biological performance [5].

This work aims to develop an intestinal tissue engineering model based on intestinal fibroblasts and epithelial cells supported by a natural biomaterial – alginate - resembling the intestinal ECM. Such intestinal tissue engineered model, with different degrees of complexity, can be used to mimic the intestinal human tissue and be further explored to correlate the permeability of model drugs with the in vivo situation. The optimized intestinal tissue is expected to be based on fibroblasts embedded in peptide-modified alginate hydrogels, following incubation for ECM production to recreate a more physiological 3D cellular microenvironment and subsequent epithelial cells deposition and differentiation, constructed on immortalized epithelial cells line Caco-2 and HT29-MTX, further differentiated with Raji B cells into M-cell like cells.

The rationale for the overall project concept stems from the idea of developing an economic tissue technology to be useful in absorption's evaluation on new oral drugs delivery.

1.2. Dissertation structure

This thesis preparation is organized into five chapters, each addressing a relevant stage within the development of the work conducted during the last months. Each chapter is built independently both theoretically and in the logical arguments construction. The remainder of this Section presents the main motivations and objective of the thesis.

Chapter 2 presents a literature review where the available knowledge about small intestinal characteristics, native ECM, hydrogel networks and intestinal 3D models are described. Several works published by different authors in the past are critically analyzed and the background for this study is therefore enriched. Chapter 3 presents the materials and methods used in the work developed. Chapter 4 covers all experimental results obtained and respective discussions.

Finally, the conclusions drawn for the entire study as well as the future improvements and the future work are provided in Chapter 5.

Chapter 2 - Literature Review

2.1. Small intestinal

The human small intestine is divided into three sections – duodenum, jejunum and ileum – and represents approximately 90% of the total absorption in the gastrointestinal tract [6].

Histologically, the gastrointestinal tissue (GI) is composed by four main layers: mucosa, submucosa, muscular and serosa, represented in Figure 1.

The Intestinal mucosa is the most internal layer and is composed of an epithelial layer, the lamina propria and the muscularis mucosae (a thinner layer of smooth muscle) [7]. The lamina propria is composed by connective tissue and provide mechanical support to the epithelium. It contains blood and lymph vessels, fibroblasts and connective tissue extracellular matrix fibers, smooth muscle cells, macrophages, mast cells, eosinophils and unmyelinated nerve fibers [8] .

This intestinal layer is characterized by the presence of villi, vascular projections of the mucosal surface that increase the available area for absorption of nutrients, covered by a single-layered epithelium, lying inside a network of blood and lymphatic capillaries. Most of cells at the surface of villi present cytoplasmic extensions, known as microvillus that increases even more the surface of absorption. Along the entire epithelial surface the microvillus form a brush-border surface [7].

Below the mucosa, a thicker layer of connective tissue constituted by nerves, blood vessels and small glandules formed the submucosa. The nerves present in this layer from a submucosal plexus [7].

The muscular layer is constituted by smooth muscle disposed in two layers, the intern circular and the external longitudinal. Between the two layers of muscle exist a nervous plexus, denoted as myenteric plexus. The submucosal plexus and the myenteric form the enteric plexus that have an important role in the regulation of movement and secretive activity [7].

The serosa, the most external layer of the GI tissue and is constituted for connective tissue that covers the interior of the walls of abdominal cavity and connected with the surrounding connective tissues to cover the major organs that contain the GI [7].

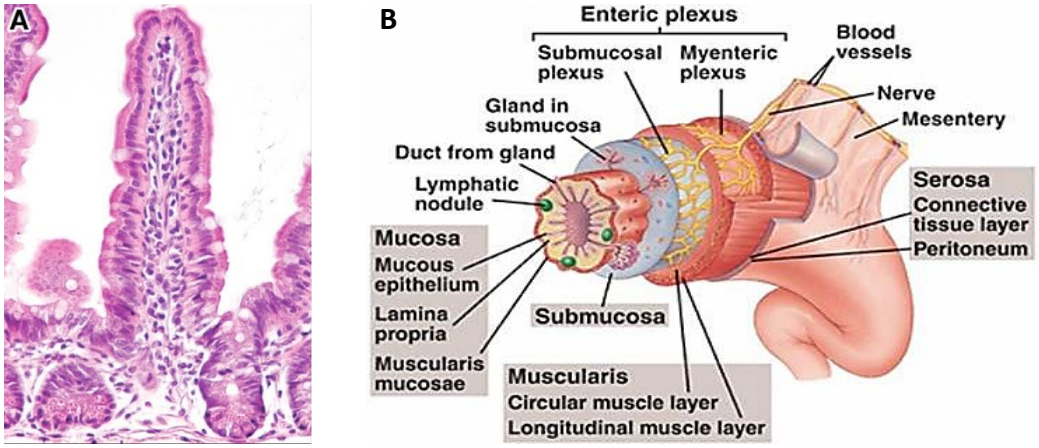

Figure 1 - A| Histology of intestinal epithelium. Staining Hematoxylin and eosin. **B| Schematic illustration of the gastrointestinal tissue** (adapted from[9,7]).

2.1.2. Intestinal cells

The cell-layer epithelium of the gastrointestinal tract represents the largest interface between the internal and external environment. The intestinal epithelium is comprised of five primary cell types, the enterocytes (absorptive cells), the enteroendocrine cells, the goblet cells, the M cells and the Paneth cells [8].

The epithelium of human intestine (see **Figure 2)** is one of the most quickly renewing tissues. The proliferation is sustained by intestinal stem cells (ISC's) and occurs at the bottom of crypt, with cell maturation occurring as they migrate along the villus axis. The crypt represents the monoclonal proliferative compartment of the intestinal epithelium and the villus the differentiated polyclonal compartment, since its cells derive from several crypts [10,11].

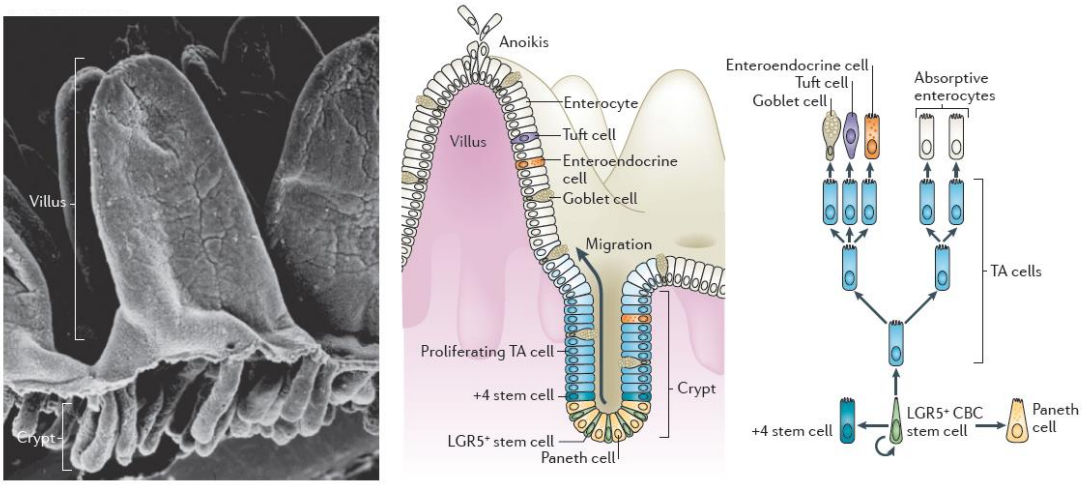

Figure 2 - Intestinal epithelium. Crypts and finger-like villis of epithelium and the location of the major differentiated cell types. Except for Paneth cells, the other cell types migrate (as clonal lineages) to the tip of the villi (adapted from [10]).

The enterocytes are the most common epithelial cell in the small intestinal lining, and are responsible for nutrients and drugs absorption [6]. In fact, the luminal surface is an important barrier to diffusion. Normally, the nutrients have to pass through enterocytes (transcellular pathway) before they reach the underlying lamina propria. The epithelial barrier function is regulated by epithelial junctional complexes, denominated as the tight junction (TJ), that surround the apical membranes of adjacent enterocytes formed an effective barrier to non-selective diffusion between the luminal contents and the underlying tissue compartments [8, 12].

This highly polarized cells derives from the embryonic intestinal endoderm and later in adult phase from intestinal stem cells [11]. Their position on the villus wall reflects their stage in the life cycle: cells on the tips of intestinal villi they undergo programmed, apoptotic, cell death and are shed from the epithelium. They are replaced at the base of the villus by stem cell mitosis [8].

Between the enterocytes, are distributed the goblet cells that represent the second largest population of intestinal epithelial cells. This population is able to secrete mucins and other proteins whose main function is to protect against microorganisms and toxins, and also lubricate the intestinal lining [8].

Driven by the Notch signaling pathway, enteroendocrine cells, having ten different subtypes, represent 1% of total epithelium. This type of cells are responsible for secreting a variety of hormones that participate in glucose homeostasis, satiety, pH balance, gall bladder contraction, gut motility and the regulation of pancreatic and pituitary hormone secretion [13,14].

In the basal portion of the intestine glands we can find the Paneth cells. They are the only differentiated intestinal epithelium cell type that migrates downward to the crypt bottom [11]. These cells play a role in the control of intestinal flora, once they are able to secrete lysozyme, a highly specific antibacterial enzyme, and other defensive proteins, which protect the intestinal luminal surface [8].

Regarding the M cells (microfold), morphologically are distinct from enterocytes, displaying poorly organized brush border with irregular microvilli at the apical domain and a basolateral cytoplasmic invagination which creates a pocket for lymphocytes and macrophages [15] (see **Figure 3**).

Microfolds are a specific epithelial cell type specialized that are confined to the epithelial region known as the follicle-associated epithelium (FAE). Overlaid by the FAE, the intestinal tissue contain organized immune inductive tissues, collectively referred to as mucosa-associated lymphoid tissue (MALT). MALT are characterized by the presence of non-encapsulated lymphoid follicles containing lymphocytes (T and B cells) and antigen presenting cells (macrophages). M cells are able to capture macromolecules, particles, and microorganisms by endocytosis and transport them to the underlying immune cells, which migrate to other compartments of the lymphoid system, where it initiates the immune response. Therefore, the M cells represent an important link in the intestinal immune defense, however, the exact role of these cells in the immune response, as well as the mechanisms of absorption and transport of particles remains poorly understood [16,17]. The M cell origin is also an issue that does not remain fully known, in fact existing two controversial theories: M cells can either derive from

stem cells or suffer a phenotypic conversion of enterocytes resultant of lymphoid environment [18].

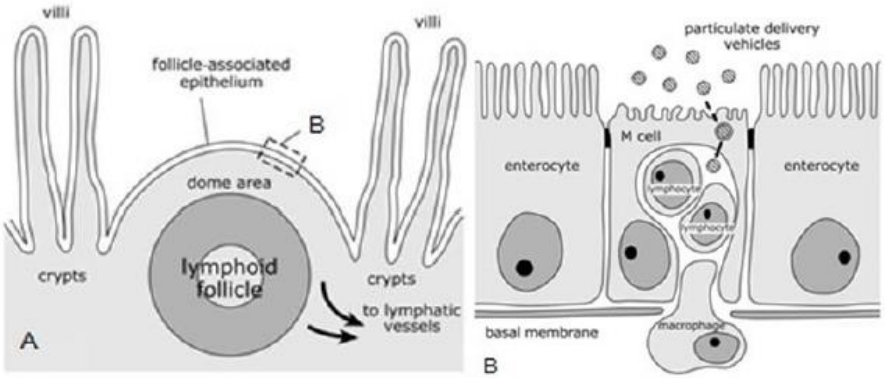

Figure 3 - Schematic illustration of intestinal sites of immune response. The lymphoid follicle is situated beneath a subepithelial dome that are below the epithelium and which is covered by the FAE. The M cell present in epithelium possess poorly organized brush border with irregular microvilli on their apical domain and a basolateral cytoplasmic invagination. (adapted from [19]).

2.1.3. Intestinal absorption

The oral route remains the most popular and acceptable route of drug administration. Along the process of absorption, the drug need to cross main barriers being the intestinal mucosa the major barrier to drug absorption [20].

After cross the mucus layer, the molecules may cross the intestinal epithelium through several functional pathways in parallel: transcellular route, paracellular route, receptor-mediated transport, carrier-mediated transport and vesicular transport [21]. In **Figure 4** is illustrated the different transport processes or absorption of a drug into the intestinal epithelium.

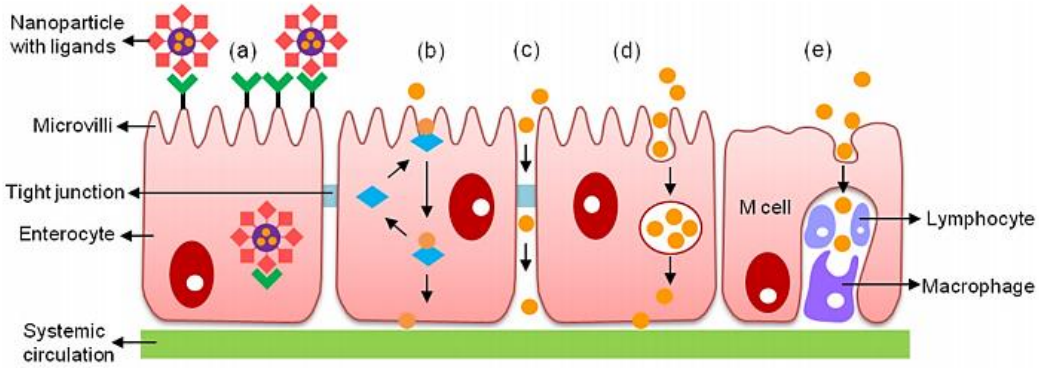

Figure 4 - Representative scheme of the transport mechanisms and pathways of a drug through the intestinal epithelium. (a) Receptor-mediated transport, (b) carrier-mediated transport, (c) Paracellular pathway, (d) Transcellular pathway, and (e) Vesicular Transport (uptake into the lymphatic circulation through M-cells Peyer's patches). (adapted from[21]).

The process of absorption occurs mostly by passive diffusion. The diffusion of molecules can occur through transcellular or paracellular route.

The transcellular route involves the passage of the particles through the cells in a process named endocytosis (uptake in membrane-bound vesicles) at the apical membrane, whereas the paracellular pathway refers to the passage of molecules between adjacent cells, using the intracellular space. Only small hydrophilic molecules (molecular weight <100-200 daltons) are absorbed by paracellular pathway and due the presence of tight junctions between enterocytes this pathway represent about 0.01% of the total intestinal mucosa surface that contribute for transport [20,22] (see **Figure 4|c-d**).

The choice of the absorption or transport route for particular compound depends on its physicochemical characteristics such as molecular weight, stereochemistry, globular size, solubility and also the characteristics of the biological membrane [20]. Lipophilic and large compounds across the biological membrane mainly by the transcellular route whereas small hydrophilic compounds and peptides tend to cross the membrane by paracellular pathway [22].

Alternatively to passive diffusion, certain proteins and peptides are transported by specific carrier present in the intestinal epithelium (see **Figure 4|b**). The transport mediated by a carrier is an energy-dependent pathway characterized by the reversible reaction between the substance being transported and the transport protein of the membrane. The molecular cross the apical domain with subsequent passive diffusion into the basolateral space [20,21]. Nevertheless, some macromolecules across the transcellular barrier through receptor-mediated transport (see **Figure 4|a**). This pathway is characterized by an initial binding the ligand to a specific surface receptor, and a subsequent receptor clustering and internalization through coated vesicles into endosomal acidic compartments. In this transportation the molecular can act either as a receptor specific ligand for surface-attached receptors or as a receptor for surface-attached ligands [21].

Finally, M cells in the FAE have been explored as a route of transport (see **Figure 4|e**). They deliver proteins and peptides to the underlying lymphoid follicles for the induction of immune response, therefore M cells represent a potential route for proteins and peptides due to their high endocytosis ability [21].

Once absorbed, the drug can be deposited in the lymphatic vessels, moved through or entrapped in the lymph nodes or transferred to the blood [23].

2.2. 3D environment

Many of the cell culture systems are performed in 2D conditions, such as tissue culture flasks, Petri dishes and micro-well plates because of the high cell viability, and convenience of use. These culture systems have remarkably improved the understanding of basic cell biology, but the disadvantages reside in the use of a 2D substrate [24]. For example, Kim, K. and collaborators demonstrated that hepatocytes, when isolated and plated onto 2D substrates, usually presents a loss of mature phenotypic character and functionality [25]. Literature has suggested and verified that the cells grown in 3D environment are more representative of what occurs naturally *in vivo*. In fact, the survival of cells inhabiting a 2D rigid substrate requires a drastic adaptation because of the lack of the unique extracellular matrix environment of each cell type.

In the human body, nearly all tissue inherently present a 3D architecture. The cells through complex physical and biochemical signals interact with the ECM, known as cell-ECM interaction, and with neighbouring cells, known as cell-cell interaction. These interactions provide a three-dimensional communication network that supports the specificity and homeostasis of the tissue, and they are essential to cell differentiation, proliferation and a range of other important cellular functions [4,6].

Two types of supporting structures have been emerged as possible forms for tissue engineering: the "solid" scaffolds, which are usually tridimensional microporous structures; and hydrogel-like matrices, which generally consist on cross-linked polymeric networks with high water contents [27].

During the past decades, artificial 3D matrices, that mimic the natural ECM, have become increasingly evident to overcome the gap between 2D cell culture and physiological tissue as they efficiently mimic in vivo situations and allow for cell–ECM interactions [28].

It is important to note that artificial 3D matrices can be divided into two areas of application: clinical and in vitro 3D modeling approaches. The clinical applications mainly consist of regenerative medicine or tissue engineering, with the objective of creating a functional implant using artificial 3D matrices [24].

The other application makes use of this type of matrices in the development of in vitro 3D model systems. Here, the aim is to perform basic research and drug development/screening, where the 3D environment will significantly improve the understanding of tissue physiology and pathophysiology. In the drug screening field, the use of 3D in vitro systems has been suggested as a potential link to bridge the gap between the monolayer cultures and *in vivo* animal model systems [4,9].

Although the 2D culture systems are still entrenched in the industry for most kind of cell-based toxicology and efficacy assays, the most recent developments and innovations demonstrate that the change from 2D to 3D cell culture for industrial purposes, as in drug research for example, is simply a question of time and 3D cell culture will surely become more applicable [29].

This review will initially present a brief description of the native extracellular matrix which has been a source of inspiration for the development of artificial matrices. A description of the

properties and characteristics of hydrogels which have been widely used as artificial cell niche to mimic extracellular matrix, is then presented.

Finally a brief report of 3D culture systems with hydrogel-like matrices is provided.

2.2.1. Native ECM

The extracellular matrix (ECM) is a nature's ideal biologic tissue engineered scaffold or biomaterial for tissue morphogenesis, maintenance and regeneration [10,11]. The complex mixture of structural and functional molecules present in ECM provides a vital 3D structure and mechanical support to the tissues and organs [30].

The ECM also provides a means to the communication between cells and their external environment, and a support or conduit for different tissue and structures, such as nerves, lymphatics, blood vessels; and also control the diffusion of nutrients from the blood to the cells [11,12]. Therefore, the ECM plays an important role in the regulation of cell behavior, like cell migration, proliferation and orientation and it is also a reservoir for signalling biomolecules that modulate processes such as vasculogenesis, angiogenesis, immune responsiveness and inflammation [10,12].

The ECM has a complex and dynamic composition, which is unique for each tissue and organ because it depends on factors like location and the physiological requirements of each physiological structure. For example, organs rich in parenchymal cells, such as the kidney, have little ECM, in contrast with tissues that have primarily structural functions, such as ligaments and tendons. The ECM of the submucosa that resides subjacent to structures rich in epithelial cells, like the mucosa of the small intestine, is disposed to be well vascularized, contain essentially type I collagen and a diversity of growth factors including epidermal growth factor (EGF) and basic fibroblast growth factor (bFGF). Whereas, the ECM of the basement membrane that resides beneath to the hepatocytes of the liver, for example, is composed of different collections of proteins including, collagen type IV and laminin [30]. Nevertheless, all the ECMs share common features [30].

The ECM is a hydrated gel-like substance rich in anionic macromolecules such as polysaccharides in the form of glycosoaminoglycans and proteoglycans [32]. Glycosaminoglycans are important components that play a critical role in binding of growth factors and cytokines and water retention. Although the amounts of cytokines and growth factors present within ECM are small, these molecules act as potent modulators of cell behaviour [33]. Within the ECM there are also present fibrous proteins such as collagen and elastin that due to the architecture and kinematics tensile strength and elasticity, respectively [32]. The collagen is the most abundance fibrous proteins within the mammalian ECM. More than twenty types of collagen have been identified with different biologic function. The different concentrations of these kinds of fibers present in matrix provide distinct mechanical and physical properties to the ECM and an ideal environment for cell growth. [33].

Adhesive proteins are also components embedded in the network, such as laminin, fibronectin or vitronectin, which bind to receptor proteins (integrin, selectins, CD44 and syndecan) present on cell surface as well as other components of the matrix [10,12].

Understanding the structure and general composition of the extracellular matrix is an important step in the development artificial 3D matrices [34].

2.2.2. Hydrogels in tissue engineering

Hydrogels are highly hydrated polymeric materials that possess a 3D structure. They are composed of cross-linked hydrophilic natural or synthetic polymer chains. The synthetic hydrogels include, for example, polylacyides/glycolides, polycaprolactone, polyhydroxyalkanoates, poly(propylene fumarates) and polyurethanes. Natural hydrogels, which are derived from plants, animals and microorganisms, include, collagen, fibrin/fibrinogen, proteins, elastin, alginate, chitosan, polysaccharides and hyaluronate [7,15].

Hydrogels can be formed with essentially any shape, size and form and the crosslinking of the polymer molecules can be achieved chemically or physically. Physically cross-linked hydrogels have H-bonding and hydrophobic forces while the chemical cross-liked are covalently bonded. These crosslinking reaction enables control of the structural integrity of hydrogels [36].

The native ECM is a hydrated gel-like substance, therefore biomaterials with hydrophilic chemistry are better choice to mimic aqueous in vivo environment. For this reason, the hydrogels, compliant and permeable structures, are one of the potential candidates to use as an artificial cell niche which resemble the native ECM [24]. Also the control of the hydrogel structure it is a critical advantage since it can improve the mechanical and biochemical properties of the hydrogels and to better mimic the native ECMs. In addition, several types of hydrogels can be cross-linked *in situ* under mild conditions and by using a variety of strategies, creating appropriate conditions for cell entrapment [35].

Over the last decade, the properties of hydrogels have made them attractive in different fields, as stem cell engineering, drug delivery, tissue engineering, cellular and molecular therapies, immunomodulation or cancer research. Nevertheless, most of these applications besides the mechanical and chemical properties, also require dynamic interactions between the surrounding matrices and the cells, providing cell compatibility [37]. Furthermore, the cell adhesion is a key factor for survival of most cell types in a tridimensional behavior and the poor cell adhesion due to the hydrophilicity of hydrogels and the lack of cell binding motifs is a drawback. To overcome these limitations some strategies have been set to improve the biological attributes of hydrogels. For example conjugating cell-binding motifs like arginine-glycine-aspartate (hereafter abbreviated as RGD) on polymer chains or coating surfaces with bioactive materials post-fabrication [24]. These techniques can be used to promote cell anchorage and interaction with the hydrogematrix.

2.2.2.1. Alginate hydrogel

Alginates are natural polysaccharides derived primarily from brown seaweed and bacteria, and is of particular interest for a wide range of applications as biomaterials due to their excellent properties in terms of biocompatibility, biodegradability, non-antigenicity, among

others [5]. Alginates have been used in particular as artificial extracellular matrix and/or in controlled delivery system for bioactive molecules and cells for tissue repair and regeneration. Alginates form viscous aqueous solutions with rheological properties that depend on the molecular weight and the concentration of the biopolymer [3,18].

From a molecular perspective, alginate is presented as a copolymer composed by two types of monomers along the polymer backbone: ß-D-mannuronic acid (M) and the α-L-guluronic (G) residues, bonded by 1→4 glyosidic linkages. The proposition and sequence of these residues are variable and can be continuously arranged to give homopolymeric blocks (MM or GG), or alternately, yielding heteropolymeric MG blocks as shown in Figure 5Figure 5. The composition, sequence and size of the different blocks, and the molecular weight of the polymer are critical factors that affect the physical properties of alginate and their hydrogels [18,19].

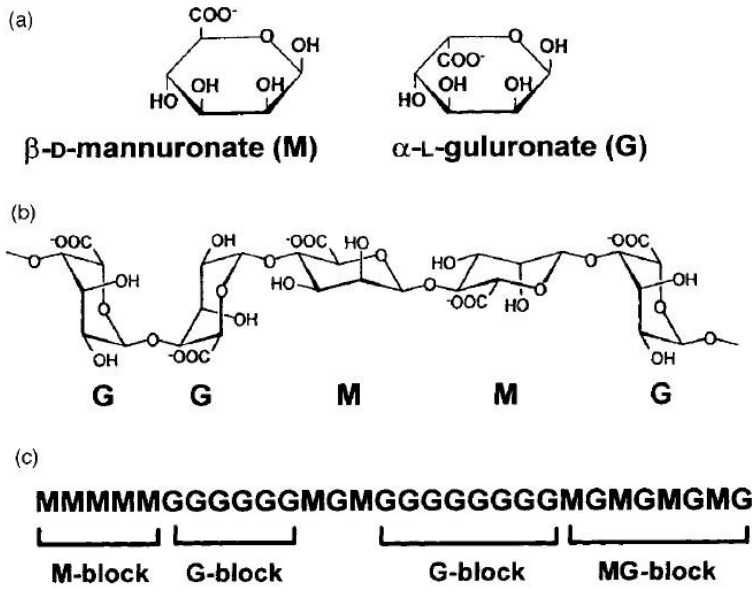

Figure 5 - Structural characteristics of alginates: A| alginate monomers; **B|** chain conformation; **C|** block distribution. (adapted from [39]).

In the presence of divalent ions, the alginate solution is ionically cross-linked between chains to form hydrogels. These ionic-crosslinking is the most common method to prepare alginate hydrogels, although others methods are employed including, phase transition (thermal gelation), cell-crosslinking, free radical polymerization and "click" reaction [5].

The process of ionic gelation of alginate solutions is related to their affinity for certain divalent ions, especially calcium ions, and the ability to establish selective links forming thermostable and insoluble gels. The selectivity of these ions is related to the ratio of G consecutive blocks, which contributes to the structural conformation acquired by diaxial link between G residues, as well as the presence of carboxyl groups in the polymer chain of each residue [39].

The alginate hydrogel formation in the presence of calcium ions is conventionally explained by the egg-box model as shown Figure 6, under which the bivalent calcium ions interact with

the carboxyl groups of the polymer G residues in adjacent chairs through ionic cross-links, resulting in a three-dimensional polymer network [39].

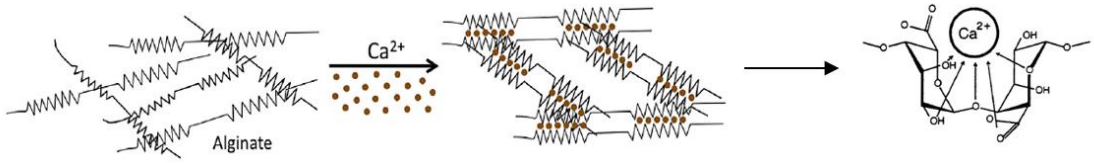

Figure 6 - The egg-box model for binding of divalent ions to homopolymeric G-blocks. (adapted from [35,39]).

In the literature, essentially two different methods for the preparation of alginate hydrogels by ionic cross-links are described: external gelation or diffusion setting and internal gelation. The external gelation is characterized by a rapid gelation process, in which calcium ions are added to an alginate solution in the form of a soluble salt such as calcium chloride ($CaCl_2$). There is an instantaneous gelation of the polymer at the contact interface with the ionized calcium ions. The gelation process continues with the diffusion of calcium ions through the gelled membrane formed. This method generally yields heterogeneous gels, which haves a higher polymer concentration at surface in relation to the core [19,20].

To achieve a homogeneous distribution of the alginate in the hydrogel, it becomes necessary to control the crosslinking velocity, as slow gelation yields a more uniform structure and a higher mechanical integrity. This can be achieved through an internal gelation method that is based on the use of an inactive source of calcium, for example, calcium carbonate ($CaCO_3$) or calcium sulphate ($CaSO_4$). The release of calcium ions is generally controlled by pH decrease caused by the addition of slow hydrolysis molecules such as glucone-δ-lactone (GDL). **Figure 7** presents schematic diagrams of the both gelation process [40].

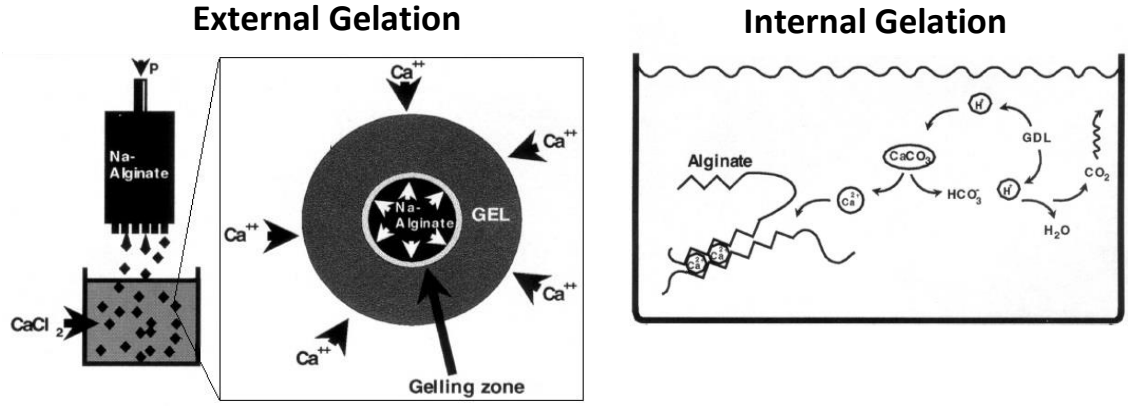

Figure 7 - Schematic diagram of external and internal gelation of alginate. (adapted from [39]).

2.2.3. 3D cell-based models

The different types of existing in vitro cell models have different degree of complexities at the level of cellular organization and behavior, providing different in vivo relevant information. The cells can be grown from simple models to complex organotypic models that are capable to reproduce the relevant functions of a tissue or organ system. Organotypic cultures are an in vitro model that often involve two or more types of cultured cells to represent in vivo-like cell heterogeneity [21,22].

These models are based on primary, immortalized or stem cell line and can use supporting matrices that allow simulating the composition of native extracellular matrix to mimic tissue or organ cultures (see **Figure 8**) [41]. In fact, for a long period of time, biomaterial studies have focused on single cells models. However, along the past few years, the use of supporting biomaterial in organotypic models show that systems better model the natural tissues, biologically and physically, through the interactions between different cell types that facilitate viability, differentiation as well as generating proteins and growth factors [26].

In the literature it has been reported different 3D culture models, including specific models for single organs, which have been established to study different systems, such as the nervous system, the skin, the liver, the respiratory system, the intestine and the heart, among others. However, here only intestinal 3D culture models will be described in more detail.

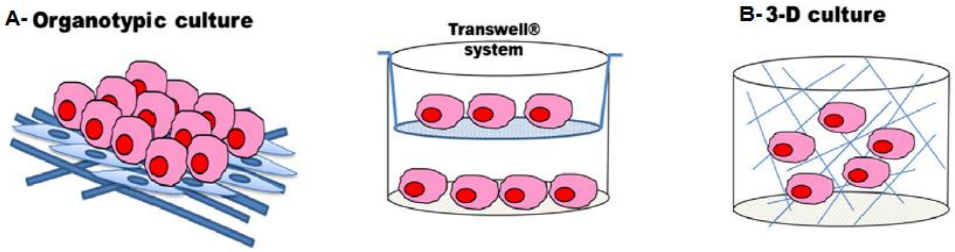

Figure 8 - - In vitro cell models. A| Examples of organotypic culture: artificial skin and co-culture on Transwell® inserts; **B|** 3-D cell culture in a supporting matrix. Adapted from [41]).

2.2.3.1. Intestinal epithelium models

Currently there is a considerable interest in the pharmaceutical industry in the development of *in vitro* human small intestinal models in order to evaluate strategies for investigating and/or enhancing the absorption of drugs. Although the conventional 2D cell system present some advantages, a significant progress has been made in the development of new 3D culture models of small intestine epithelium by using microfabrication, biomaterials, microfluidics and tissue engineering principles, in the past five years [43].

With the development of biomaterial fabrication techniques it began to be possible to replace the planar membrane where the cells were traditionally seeded by more advanced bio-structures, such as hydrogels, which are able to mimic some of the features of human small

intestinal villi. As a result, Wang, Li and collaborators developed a biomimetic intestinal culture system composed by a collagen membrane substrate with a human small intestine crypt-like topography that was coating with ECM proteins (laminin or fibronectin). Enterocyte-like cells were seeded on top of the collagen membrane, and cultures for 21 days (**Figure 9**). This study showed that the crypt-like topography might affect tight junctions of the Caco-2 monolayer in a short term, and that the effects on phenotype of intestinal epithelial cells are gradually diminished with prolonged time of culture [44].

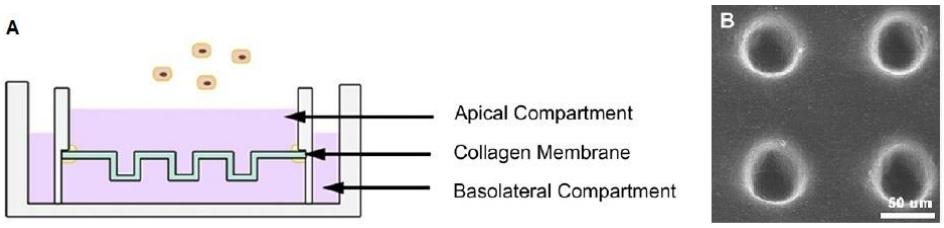

Figure 9 - Schematic illustration of intestinal epithelial culture system in a collagen membrane. A| 3D system with a collagen membrane and **B|** Back view of collagen membrane. (Adapted from [44]).

In another study, it was recently demonstrated that combination of laser ablation and sacrificial molding techniques can be used to develop a collagen hydrogel structure mimicking the density and size of the human jejunal villi. Enterocyte-like cells (Caco-2 cells) were seeded onto the structure and cultured for 3 weeks. As shown in **Figure 10**, remarkable similarities are observed between Caco-2 cells on collagen scaffold and the human jejunal villi. The cells were able to proliferate, invaded and covered the collagen villi. This method of microfabricated hydrogels offers several advantages and is a promising method for the construction of in vitro tissue models [45].

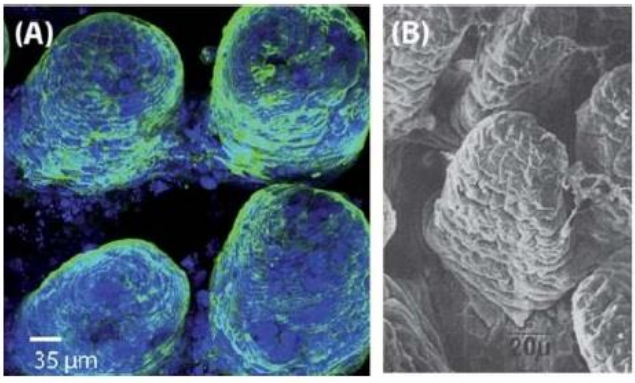

Figure 10 - A| Confocal microscope image of Caco-2 cells on collagen scaffold, after staining for actin (green) and nucleic acid (blue). B| SEM image of human jejuna villi. (Adapted from [45]).

Latter, the same group developed a well-plate insert in order to simulate the villi space at 25 villi/mm^2 based on the existing insert and this way facilitate the commercialization (see **Figure 11**) [46]. The enterocyte-like cells seeded on top of the collagen villous exhibited differentiation gradients along the villous axis: near the top of the villus the cells were more

polarized and columnar than cells presents near the bottom of the villus, correlating with the process of differentiation that is observed in vivo in human intestinal epithelium [35,36].

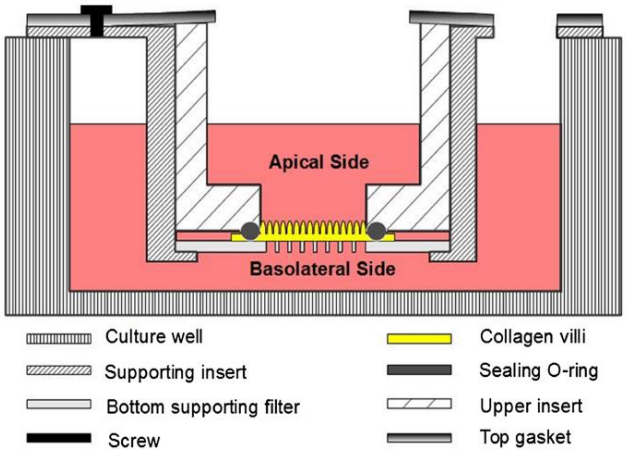

Figure 11 - Schematic illustration of the insert design. (Adapted from [46]).

The intestinal epithelium has an important function not only in the absorption process, but also in in inflammatory response. To study intestinal inflammatory process, another type of 3D model was developed by Leonard and collaborators, consisting in a monolayer of enterocyte-like cells (Caco-2) overlying a collagen matrix containing immune components (dendritic cells and macrophages) (see **Figure 12**) [47].

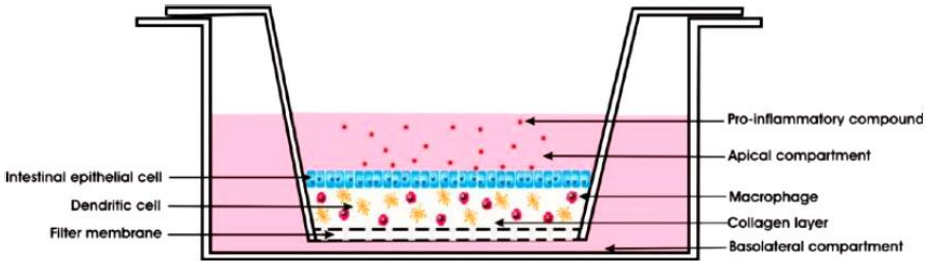

Figure 12 - Schematic illustration of the 3D cell culture system. (Adapted from [47]).

The results of this study show that cultivation of macrophages and dendritic cells together with the epithelial cells, over 21 days, allows the differentiation of these cells toward the phenotype intestine-like characteristic.

Regarding the epithelial cells, even in the presence of immune cells, 3 weeks of culture is necessary for the monolayer formation and the results show a similar developed of tight junction in compare to the Caco-2 monolayer. When occurs the stimulation with addition cytokine IL-1ß, the TEER value decreased, however, after removal stimulation, the TERR value increased gradually and recovered after 7days.

Other aspect observed in this model, its IL-8 protein release into the medium in response to the stimulation with IL-1ß. The amount was significantly higher in comparison to the Caco-2

monolayer model. This increase of pro-inflammatory activity can reflected the activity of the dendritic cells and macrophages. To support this ideas, was observed by histological cut and by confocal laser scanning microscopy image, an increased invasion of immune cells to the apical side in inflamed model in comparison to healthy model (see **Figure 13**).

Although the collagen matrix does not present the typical villi-like topography of the small intestine, the incorporation of macrophages and dendritic cells in the collagen matrix makes this 3D cell culture model a power in vitro tool for studying inflammatory bowel disease [47].

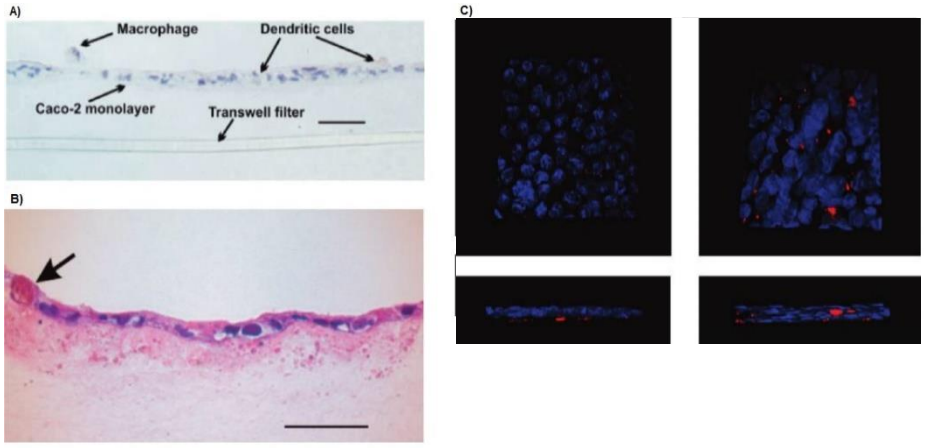

Figure 13 - A| Monolayer of Caco-2 cells on top of the collagen layer with the nucleus in blue. Hematoxylin Staining **B|** The collagen layer contained the immuno cells (macrophages and dendritic cells colored red) and this cells were also found into the cell monolayer or on top of it. Acid phosphatase Staining. **C|** Confocal laser scanning microscopy image of 3D culture, detected the immuno cells through the intestinal epithelium cells (blue), from their auto fluorescence (red), but can not be distinguished. (Adapted from [47]).

Chapter 3 - Materials and Methods

3.1. Materials

Six grades of sodium alginate from several algal sources were purchased from ISP industries, U.S.A. and Germany; and Sigma-Aldrich, Canada. These can be classified into three main groups according to their molecular weights, and content in acid Mannuronic (M-rich) or acid guluronic (G-rich).

The M-rich alginates used were Manucol LD, Keltone (LV and HV); while the G-rich alginates used were Manugel (LBA and DMB) and Alginic acid sodium. Some physic-chemical properties of the different types of alginate used in this study are described in **Table 1**.

For the cell culture experiments an ultrapure alginate M-rich (Pronova UPLVM) purchased from NovaMatrix was used. Some of its physic-chemical properties are described in **Table 2**.

Sodium chloride (NaCl) was purchased from Merck ®, while calcium carbonate ($CaCO_3$) was purchased from Fluka®. Tris(hydroxymethyl)aminomethane (Tris) was purchased from AmResco®.

Calcium chloride ($CaCl_2$), D-glucono-d-lactone (GDL), 1-ethyl-(dimethylaminopropyl)-carbodiimide (EDC), MES and HEPES buffer salt, Hydroxylamine, PolyHEMA were purchased from Sigma. N-Hydroxy-sulfosuccinimide (Sulfo-NHS) was purchased from Thermo Scientific. Peptide (glycine)4–arginine–glycine–aspartic acid–serine–proline (RGD) was purchased from Genscript. Dialysis Tubing (MWCO 3500 membrane) was purchased from Fisher.

Dulbecco's Modified Eagle's Medium (DMEM) was purchased from Lonza. Non-essential aminoacids (NEAA) was purchased from Biochrom. Trypan Blue, 0.05% Tripsin/EDTA, Hanks Balanced Salt Solution (HBSS), DMEM without phenol red were purchased from Gibco®, while Fetal Bovine Serum (FBS) and Penicillin/Streptomycin were purchased from BioWest. 24-well Transwell® permeable support (PET membrane and 3µm pore size) were purchased from BD Biosciences. Ethylenediamine tetraacetic acid (EDTA), Resazurin, Bovine Insulin, Triton X-100, DAPI, Fluoroshield™ mounting medium, picrosirius red and Propidium Iodide (PI) were purchased from Sigma.

Calcein-AM was purchased from Invitrogen. Anti-human vimentin antibody was purchased from Santa Cruz Biotecnology. PerCP-Cy™5.5 mouse anti -human Alkaline Phosphatase antibody was purchased from BD Pharmingen. Rabbit anti-fibronectin polyclonal antibody was purchased from Sigma. Donkey anti-mouse AlexaFluor 488, AlexaFluor 594 F(ab')2 fragment of goat anti-rabbit, secondary antibodies were purchased from Molecular Probes-Invitrogen.

Table 1- Physicochemical properties of each type of alginate, as provided by the manufactures [48]–[52].

	Alginate Type	Viscosity 1% (mPa.s)	Content (%)		M/G Ratio	Designation
			Mannuronic acid)	Guluronic acid		
Low Molecular weight	Manugel LBA	3-4	37	63	0,59	LMW-G
	Manucol LD	10	60	40	1,50	LMW-M
Medium Molecular weight	Keltone LV	50	60	40	1,50	MMW-M
	Alginic acid sodium	Low (250 a 2%)	39	61	0,64	MMW-G
High Molecular weight	Manugel DMB	300	37	63	0,59	HMW-G
	Keltone HV	400	60	40	1,50	HMW-M

Table 2 - Physicochemical properties of PRONOVA UPLVM alginate, as provided by the manufacture [53].

Alginate Type	Apparent Viscosity (mPa.s)	PH	Content (%)		Designation
			Mannuronic acid	Dry matter	
PRONOVA UPLVM	20-200	5.5-8.5	≥ 50	≥ 85	UPLVM

3.2. Alginate characterization

3.2.1. Determination of moisture content

The moisture content of different types of alginate were determined by freeze-drying and infrared radiation.

For the freeze-drying, the different sodium alginate powders were weighed and dissolved in 50 mL of deionized water at room temperature (RT) to form aqueous solutions with a concentration of 1% (w/v). Then, 25 mL of each solution were transferred to previously weighted falcon tubes, which were then frozen at -80 °C for 24 hours in a *Forma 900 serie* ultrafreezer (Thermo Scientific; U.S.A.). After the freezing process, the samples were lyophilized by using *Freezone*6 freeze dry system (Labconco, U.S.A.). During freeze-drying, the temperature was kept at -55 °C and the process lasted about 72 hours. After freeze-drying, the falcon tubes were rigorously weighed, and by the difference in weight it was possible to determine the moisture content for each type of alginate.

Regarding infrared radiation technique, 1 gram of each alginate powder were weighed by using *AND MX-50* moisture balance (A&D Company, Limited; Japan). This type of balance has

an infrared radiation that penetrates the sample and is converted in heat molecular vibration and the water content in the sample is eliminated by evaporation.

Therefore, the difference in weights, the weight before and after radiation, allows to determine the percentage of humidity present in the alginate samples.

3.2.2. Formation of alginate hydrogel matrix

The alginate hydrogel matrices were prepared by internal gelation as previously described [15,34]. A 1%, 2% and 3% (w/v) alginate final concentration was defined for the rheometry experiments. Sodium alginate powder was weighed and dissolved in 0.9% (w/w) NaCl, at RT, to form aqueous solutions with initial concentration of 2%, 3% and 4% (w/v), respectively. $CaCO_3$ in combination with GDL was used as source of calcium ions to initiate internal gelation.

The quantity of Ca^{2+}, and consequently the $CaCO_3$, required for the alginate solution gelation was determined taking into account the number of carboxyl groups (COO^-) present on consecutive G residues. The Ca^{2+}/COO^- molar ratios of 0.288; 0.5; 0.65 and 0.75 were tested for all types of alginates and for the three concentrations defined. The molar ratio of $CaCO_3$/GDL was set at 0.125.

Calcium carbonate aqueous suspension (prepared in 0.9% (w/w) NaCl) was added to sodium alginate solutions, mixed and vortexed until homogenization. The gelling process was triggered by adding a fresh aqueous solution GDL, prepared by dissolving in 0.9% (w/w) NaCl. Then, 80µL/disc of the hydrogel precursor solution were transferred to QGel casters to form circular discs. Gel formation continued in incubator at 37 ºC under a 5%CO_2 humidified atmosphere for 1h. Thereafter, the hydrogels discs were transferred into a 24-well-plate containing 500µL of pre-warmed culture medium (DMEM with HEPES buffer), for 1h. The medium was subsequently replaced for fresh medium.

For the 3D culture studies, hydrogels loaded with cells were prepared with previously combined the cells with the hydrogel precursor solution before triggering gelation, as described in **Section 3.3.2.**

In **Figure 14**, a similar procedure is schematized, used, in this case, to prepare polyethylene glycol (PEG) hydrogels.

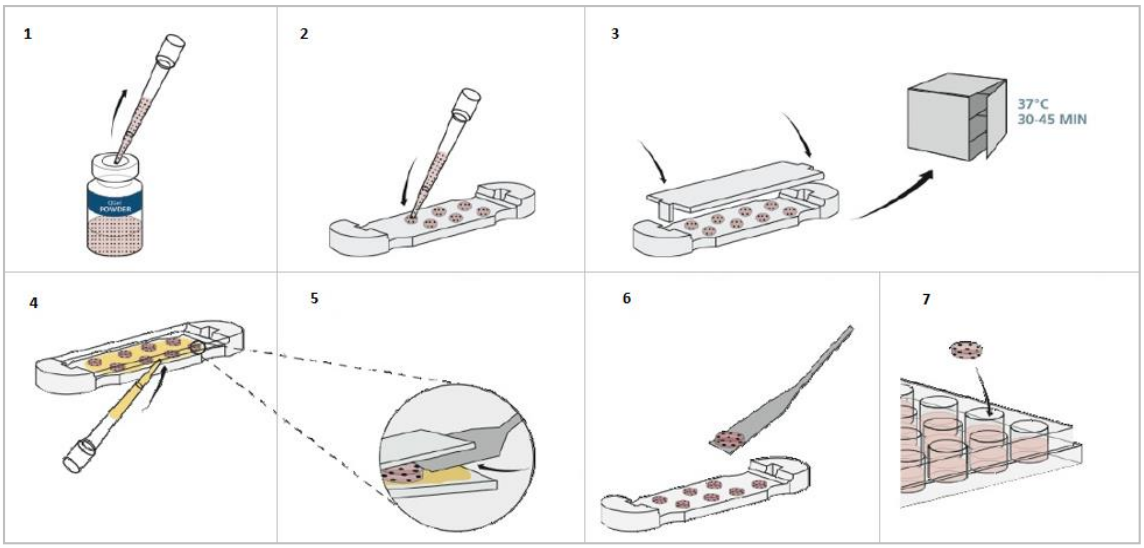

Figure 14 - Preparation of PEG hydrogels in a QGel caster: 1-2| a prefined volume of the hydrogel precursor solution is transferred to the gel caster; **3|** the gel caster is carefully closed and placed in an incubator at 37°C in a humid atmosphere for 1h; **4-5|**culture medium is applied around the discs and then the top of the gel caster is slowly withdrawn; **6-7|** PEG discs are carefully transferred into a well-plate containing pre-warmed culture medium (adapted from [55]).

3.2.3. Rheometry experimental set

In order to understand the influence of different molecular weights and the ratio of G vs. M groups on the properties of alginate hydrogels, oscillation rheometry experiments were carried out using a Kinexus Pro rheometer (Malvern Instruments, Malven, U.K.).

For the alginate hydrogels assessment, the parallel plates geometry was used, and the alginate samples with a diameter of 4mm were previously punched from the original discs to fit the geometry. The height of the gels was measured with a caliper. This step is necessary to establish the distance of the plates (top and bottom geometry), which is defined according to the height of the disc with a compression of 10% to avoid slippage.

All measurements were performed at 37ºC and in humid environment. Stress sweeps, at a frequency of 0.1Hz were first performed, for all the tested conditions, to determine the linear viscoelastic region (LVR), where the dynamic storage modulus (G') and loss modulus (G") are independent of the strain amplitude. Frequency sweeps, at a frequency of 0.01-10Hz were then performed within the LVR. The values of the storage modulus, G', viscosity modulus, G", and the phase angle, δ, for all the conditions presented in **Figure 18** were obtained at frequency at ranging 0.05-0.4Hz. Samples were analyzed in triplicate.

3.2.4. Degree of swelling

The swelling ratio of alginate hydrogels, was calculated as described in [56]. Immediately after crosslinking, the alginate hydrogels, for all concentrations with Ca^{2+}/COO^{-} molar ratios of 0.5, were placed in culture medium (DMEM with HEPES buffer) at 37ºC for 1h, freeze-dried in BenchTop Pro (SP Scientific; U.S.A.) and weight.

Assuming that the matrices swells uniformly in all directions, the swelling ratio can be defined as a ratio of the weight of swollen hydrogel to the weight of dry hydrogel. Therefore the swelling ratio (q_F) was calculated from the following equation:

$$q_F = \frac{\text{mass of gel after 1h incubation}}{\text{mass of gel after freeze-drying}}, \quad (1)$$

3.2.5. Chemical modification of alginate with peptides

HMW-M alginate and Pronova UPLVM sodium alginates were chemical modified with the cell-adhesion peptide RGD, using carbodiimide chemistry as previously described [57],[58].

Sodium alginates solution (1% (w/v)) in MES buffer (0.1M MES, 0.3M NaCl) were prepared and stirred overnight (ON), at 4 ˚C. Thereafter, Sulfo-NHS and EDC were sequentially added to the solution at a molar ratio of 1:2 per gram of alginate, followed by RGD peptide (16.7mg per gram of alginate). Blank solution were prepared without the addition of RGD peptide. After stirring for 20h at RT, the reaction was quenched with hydroxylamine (18mg per gram alginate) and the non-reacted species were separated from the polymer by dialysis (MWCO 3500 membrane) against decreasing salt solution of deionized water and NaCl for 3 days, changing the solution 2-3 times per day.

After dialysis, activated charcoal (0.5g per gram alginate) was added to the modifier alginate solution and stirred for 1h. Then, the solution was centrifuged, for 1h, at 27000 rcf, at 25 ˚C and filtered off using a steriflip. The purified solution was lyophilized and the RGD-alginate was stored at -20 ˚C until used.

3.2.6. Quantification of peptide-modified alginate

The yield of the chemical modification of alginate with RGD peptide was quantified using the BCA Protein Assay, as previously described [59].

A solution (1% (w/v)) of peptide-grafted alginate in deionizer water was prepared. Also, a set of RGD solution at concentration ranging 0 to 1 mg/mL (dissolved in 1% (w/v) blank solution at concentration of 1%) were prepared to use as standards in order to set a calibration curve. Thereafter, the BCA reagent was added to the samples and incubated at 37 ˚C, for 30 minutes in the dark. After incubation, the absorbance was read at 540nm in a microplate reader (Biotek Synergy MX). The efficiency of the reaction and the amount of RGD grafted was calculated by using the standard curve and taking into account the amount of peptide added in the coupling reaction. All measurements were made in triplicate.

3.3. Cell culture studies

3.3.1. Cell lines and cell culture conditions

C2BBe1 clone of Caco-2 cell line, Raji B and CCD18-Co cell lines were from American Type Culture Collection (ATCC, USA). HT29-MTX cell line was kindly provided by Dr. T. Lesufleur (INSERM U178, Villejuif, France).

CCD18-Co cell grown in 75 cm2 tissue culture flasks in DMEM basal medium supplemented with 20% (v/v) inactivated FBS, 1% (v/v) of NEAA and 1% of antibiotic/antimitotic mixture (final concentration of 100 U/mL Penicillin and 100 U/mL of Streptomycin).

C2BBe1, HT29-MTX and Raji B cells grown separately in 75 cm^2 and 25 cm^2 tissue culture flasks in DMEM basal medium supplemented with 10% (v/v) of inactivated FBS, 1% (v/v) of NEAA and 1% of antibiotic/antimitotic mixture (final concentration of 100 U/mL Penicillin and 100 U/mL of Streptomycin).

At confluence, the three adherent cells were washed with phosphate buffer saline (PBS), treated with 0.05% Trypsin/EDTA for 5 minutes to release cells from the flask, pelleted by centrifugation at 1200 rpm for 5 minutes and finally re-suspended with fresh medium and seeded with the desired cell density.

Raji B (suspension cells), at confluence, were removed from the culture flasks and pelleted by centrifugation at 1200 rpm for 5 minutes and finally re-suspended with fresh medium and seeded with the desired cell density.

Cells were routinely maintained in an incubator (CellCulture® CO2 Incubator, ESCO) at 37°C under a 5% CO2 humidified atmosphere.

For all experiments CCD18-Co cell line was harvested between passage number 9 to 20, C2BBe1 cell line between passage number 9 to 20, HT29-MTX cell line between passage number 9 to 20 and Raji B between passage number 9 to 20.

3.3.2. 3-D culture of CCD18-Co cell within alginate matrices

For immobilization within alginate hydrogel, the alginate gel precursor solutions were prepared at final concentrations 1% (w/v) (RGD densities of 155 μM).

CD18-Co cells were trypsinized when reached confluence. After centrifugation and discarding of the supernatant, cells were homogeneously mixed at different densities (D1=$1 \times 10^6 \mathrm{cells/mL}$ and D2=$5 \times 10^6 \mathrm{cells/mL}$) with alginate solutions and crosslinking agents (CaCO3/COOH molar ratio of 0.5 and CaCO3/GDL molar ratio of 0.125) as described on **section 3.2.2.**

The gel precursor solutions was pipetted (70ul per well) into the apical side of a 24 Transwell® insert or into each well of a pHEMA-treated 96 suspension well culture plate for crosslinking, at 37 C under 5% CO2 humidified atmosphere during 40 minutes.

After in situ crosslinking, DMEM basal medium supplemented with 10% (v/v) of inactivated FBS, 1% (v/v) of NEAA and 1% of antibiotic/antimitotic mixture (final concentration of 100 U/mL

Penicillin and 100 U/mL of Streptomycin), was added to CCD18-Co-laden hydrogel and cultured during 21days and medium was changed every three days. During culture, cell-laden matrices were maintained in an incubator at 37°C under a 5% CO2 humidified atmosphere.

As a control, cells were entrapped within alginate without RGD and kept under the same conditions. For the different cell studies three hydrogel matrices were analyzed for each condition.

3.3.3. Cell viability, metabolic activity and morphology

In order to determine the optimal density of CCD18-Co intestinal myofibroblasts, different cellular densities ($1 \times 10^6 \text{cells/mL}$ and $5 \times 10^6 \text{cells/mL}$) were evaluated regarding their viability, metabolic activity and morphology.

Cell viability was analysed using the live/dead fluorescence viability assy, as previously reported [60]. At day 21, the cell medium was aspirated from the 96-well and the cell-loaded matrices were wash twice with pre-warmed DMEM without phenol red. After washing, samples were protected from the light and incubated with 3μM calcein-AM (live cells), and 4 μM propidium Iodide (dead cells) for 45min at room temperature. Afterwards, the supernatant was replaced by fresh DMEM without phenol red and the samples were immediately examined by confocal laser scanning microscopy (Leica SP2AOBS, Leica Microsystems) and treated using ImageJ program.

Cell metabolic activity was conducted using the resazurin fluorescent assay, as previously described [60]. At different time points (7, 14 and 21 days), cell-loaded matrices were incubated with 20% (v/v) pre-warmed resazorin solution in culture medium, for 2h at 37°C. After incubation, 100μl of the supernatant was collected to a 96-well plate black with clear botton and immediately quantified by measuring the relative fluorescence units (RFU) using a microplate reader (Biotek Synergy MX) set at 530/590 nm (excitation/emission wavelength, respectively). All measurements were made in triplicate and the results were normalized by subtracting the negative control (without cells).

The CCD18 cell morphology was assessed by labeling the intermediate filaments of fibroblast with vimentin antibody, as previously reported [61]. After 21 day of culture, the CCD18-Co-loaded matrices were recovered and washed twice with pre-warmed TBS-Ca (tris-buffered saline, 50mM Tris in 150mM NaCl, pH 7.4, with 7.5 CaCl2). Cell-loaded matrices were fixed with 2% (w/v) paraformaldehyde in TBS-Ca for 15 minutes at RT and permeabilized with 0.2% (v/v) Triton X-100 in TBS-Ca for 7 minutes at RT. In order to block non-specific binding, the cell-loaded matrices were incubated with TBS-Ca containing 0.05% (v/v) Tween-20 and 10% (v/v) FBS for 30 minutes in a humidified chamber. Then, without wash, blocking solution was removed and samples incubated during 2 hours at RT with a mouse anti-human vimentin primary antibody diluted (1:100) followed by secondary antibody donkey anti-mouse AlexaFluor488® (1:1000) during 1 hour at RT, both diluted in TBS-Ca containing 5% (v/v) FBS. Finally, the matrices were counterstained with DAPI diluted 1:1000 in TBS during 5 minutes. Fluorescence-labelled matrices were imaged by confocal laser scanning microscopy (Leica SP2AOBS, Leica Microsystems) and treated using ImageJ program.

3.3.4. Immunocytochemistry staining

After 21 day of culture, the CCD18-co-loaded matrices were evaluated regarding expression of ECM components, namely fibronectin.

The procedure was performed as previously reported [60,61]. The cell-loaded matrices were recovered and washed twice with pre-warmed TBS-Ca, and fixed with 4% (w/v) paraformaldehyde in TBS-Ca for 20 minutes at RT. Therefore, the matrices were processed automatically in a Spin Tissue Processor STP120 (Thermo Scientific, Germany), where the samples were dehydrated using a series of ethanol solutions of increasing concentrations for 10 minutes each, followed by a diaphanization using twice a ClearRite 3 for 10 minutes. The cell-loaded matrices processing was finished by embedded in liquid paraffin for 2 hours. Thereafter, the matrices were orientated according the plane of cut.

Thereafter, paraffin-embedded sections (3µm) were recovered using a Leica RM2255 microtome (Leica Biosystems, Germany), de-paraffinized in xylene for 10 minutes and rehydrated with a series of ethanol solutions of decreasing concentrations and finishing with TBS-Ca, during 5 minutes in each solution. Sections were fixed with 0.2% (w/v) paraformaldehyde in TBS-Ca for 20 minutes at RT and permeabilized with 0.2% (v/v) Triton X-100 in TBS-Ca for 10 minutes at RT. In order to block non-specific binding, the cell-loaded matrices were incubated with 1% BSA for 30 minutes in a humidified chamber. Then, without wash, blocking solution was removed and section incubated during 2 hours at RT with a rabbit anti-human fibronectin primary antibody (1:400) followed by secondary antibody goat anti-rabbit AlexaFluor 594 F(ab')2 fragment (1:1000) during 1 hour at RT. Finally, the matrices were counterstained with DAPI diluted 1:1000 in TBS during 5 minutes. Fluorescence-labelled matrices were imaged by confocal laser scanning microscopy (Leica SP2AOBS, Leica Microsystems) and treated using ImageJ program.

3.3.5. Histological analysis: Hematoxylin and eosin and Picrosirius red

After 21 day of culture, the CCD18-co-loaded matrices were embedded in paraffin to observe the CCD18-co spatial distribution within 3D matrices and also the expression of ECM components, namely collagen. The procedure was performed as previously reported [60]. Paraffin sections of the different samples were obtained as already described in the previous section.

Briefly, sections were de-paraffinized in xylene and dehydrated through a series of ethanol to TBS-Ca for 2 minutes each, following the staining with Gill's haematoxylin II for 5 minutes. After that, the sections were washed in tap water for 2 minutes, following dehydration through graded alcohols for 2 minutes each. Sections were counterstained with Eosin for 3 minutes and sections were dipped in absolute alcohol 3 quick times.

For picrosirius red, well-known method to stain collagen in histology, the sections were de-paraffinized, dehydrated and staining with picrosirius red for 1h, following washed in 0.01M

HCl solution. Finally, all sections were de-paraffinized in xylene three times and mount in mounting medium. Samples were visualized using optical microscope (Axioskop, ZEISS) and treated using ImageJ program.

3.3.6. Monolayer *in vitro* cell model

Monoculture of C2BBe1, co-culture of C2BBe1/HT29-MTX cells and a triple co-culture C2BBe1/HT29-MTX/Raji B cells were performed as previously described [4].

C2BBe1 monolayer (**Figure 15|A**) was prepared by seeding C2BBe1 at a density of 1×10^5 cells/cm2 on the apical chamber of 24-well Transwell inserts. These cultures were maintained for further 21 days and medium was changed every three days.

Dual co-culture of C2BBe1/HT29-MTX cells (**Figure 15|B**) was prepared by seeding C2BBe1 and HT29-MTX cells on the apical chamber of 24-well Transwell inserts at final density of 1×10^5cells/cm2 (90:10 proportion), as previously optimized [4]. Cells were maintained in the same conditions as the monoculture and the culture medium was changed two a three times a week.

The triple co-culture model of C2BBe1/HT29-MTX/Raji B cells (**Figure 15|C**) was performed as described above on the Caco-2/HT29-MTX co-culture with the addition of 0.7×10^5cells/24-well Raji B lymphocytes in the basolateral compartment.

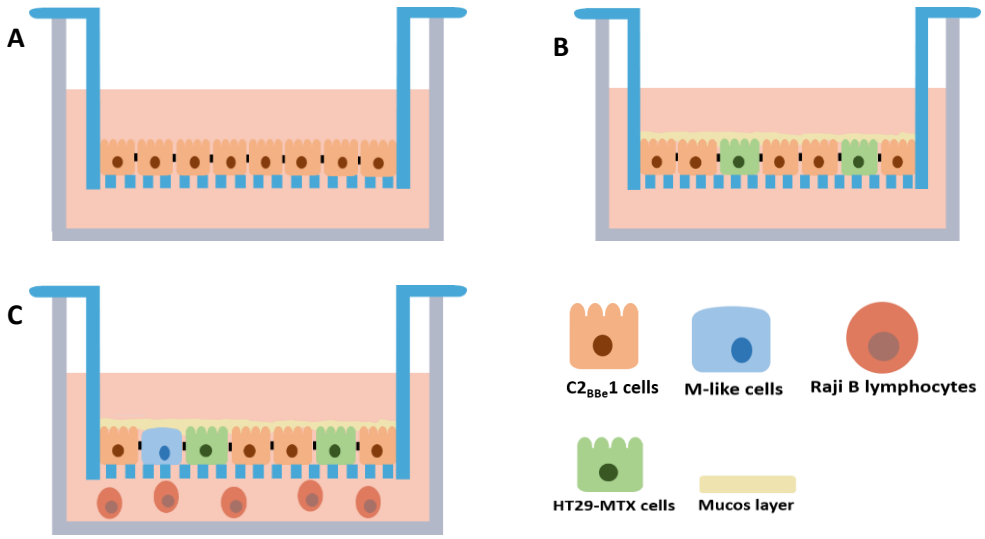

Figure 15 - Schematic illustration of monolayer in vitro models: **A|** $C2_{BBe}1$ monolayer; **B|** Dual co-culture of $C2_{BBe}1$/HT29-MTX cells; **C|** Triple co-culture model of Caco-2 clone $C2_{BBe}1$/HT29-MTX/Raji B cells.

3.3.7. Tridimensional *in vitro* model

To explore the behavior and the membrane integrity of epithelial cells on top of RGD-alginate hydrogels, a tridimensional in vitro model with C2BBe1 monolayer was performed

(**Figure 16**). The alginate gel precursor solutions were prepared at different polymer concentrations (1%, 1.5% and 2% (w/v)) and RGD densities (155, 200 or 300 μM).

As previously described on section 3.2.2, with the exception of CCD18-Co cells, the RGD-alginate solution was combined with crosslink agents (GDL and CaCO3) with final concentration of 1%, and the mixture was pipetted into the apical side of a 24-well Transwell inserts. After in situ crosslinking (40 minutes at 37°), fresh culture medium was added to hydrogel layer and incubated at 37ºC (**Figure 16|1**). In the following day, $C2_{BBe}1$ cells were added over the layer of hydrogel at different concentration (D_1=$1 \times 10^5 \mathrm{cells/mL}$; D_2=$2 \times 10^5 \mathrm{cells/mL}$ and D_3=$4 \times 10^5 \mathrm{cells/mL}$). Cells were maintained in the same conditions as the monoculture and the culture medium was changed two a three times a week.

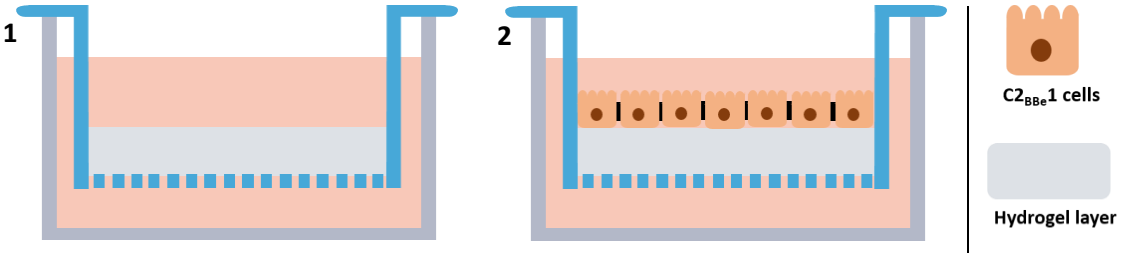

Figure 16 - Schematic illustration of the tridimensional $C2_{BBe}1$ model: 1| hydrogel layer in a Transwell system; **2|** Hydrogel/C2BBe1 model.

3.3.8. Transepithelial electrical resistance (TEER)

To monitor the evolution of confluence and membrane integrity of all the cultures, the transepithelial electrical resistance (TEER) of each model was measured using a voltohmmeter Millicell® ERS-2 (Millipore, USA) with STX3 electrode for 3D model and STX1 electrode for 2D models (world Precision Instruments, Sarasota, FL) every time that medium was replaced. Electrodes were placed on the apical and basolateral sides of Transwell insert and the monolayer resistance were obtained by subtracting the resistance value of the empty Transwell® insert from the total resistance, and expressed in ohm per area of the insert ($\Omega.cm^2$).

3.3.9. Drug transport assay

Permeability studies were performed in order to determine the permeability of the *in vitro* models developed, using insulin as model drug.

As previously described [4], culture medium was removed from both compartments of Transwell system and the cells membranes were washed twice with pre-warmed TBS-Ca. After that, new TBS-Ca was replaced and equilibrated for 15 minutes at 37˚. Transwell insulin absorption were run at 37˚C, during 4h with 200μL of 100μg/mL of insulin prepared in HBSS in the apical side and 700 μL of HBSS in the basolateral side. At different times, 100μL was collected of basolateral side after monitored the monolayer integrity by TEER measurement.

The insulin concentration of each sample was further determined by reverse HPLC-UV on a Merck-Hitachi LaChrom HPLC instrument (Merck). The HPLC system was equipped with a XTerra RP-18 column, 5 µm particle size, 4.6 mm internal diameter × 250 mm length (Waters) and a LiChrospher 100 TP-18, 5 µm particle size guard column (Merck) [62]. All experiments were run in triplicate at room temperature and the total area of the peak was used to quantify insulin. The apparent permeability (P_{app}) was calculated from the measurement using the following equation:

$$P_{app} = \frac{\Delta Q}{A \times C_0 \times \Delta t}, \quad (2)$$

, where C_0 is the initial concentration in the apical compartment (µg/mL), A is the surface area of the insert (cm^2), Δt is the time in which the experiment occurred (seconds) and ΔQ is the amount of compound detected in the basolateral side (µg).

After permeability studies, apical-basolateral flux was assessed using 4 kDa Fluorescein Isothiocyanate – Dextran molecule (FITC-Dextran), in order to evaluate the final integrity state of the models. At the end of transport experiments with insulin, the solutions present on Transwell was removed and the cells membranes were washed twice with pre-warmed TBS-Ca.FITC-Dextran assay were run at 37˚C, during 1h with 200µL of 200µg/mL of FITC-Dextran prepared in HBSS in the apical side and 700 µL of HBSS in the basolateral side. After this period, a sample was collected from the basolateral side and transferred to a 96-well plate black with clear botton and immediately quantified by measuring the relative fluorescence units (RFU) using a microplate reader (Biotek Synergy MX) set at 485/530 nm (excitation/emission wavelength, respectively). All measurements were made in triplicate and the fluorescence values were normalized by subtracting the blank and the concentration of FITC-Dextran was calculated by using a standard curve. The amount of transported 4 kDa FITC-Dextran was expressed by percentage of rejection, using the following equation:

$$\%\text{Rejetion} = \frac{1 - \text{RFU}_{\text{Basolateral}}}{\text{RFU}_{\text{Apical}}} \times 100 \quad (3)$$

3.4. Statistical analysis

The results are expressed as mean ± standard deviation (SD) and n=3. Statistical analyses were performed using GraphPad Prism 5 software.

One-way analysis of variance (ANOVA) followed by Tukey's multiple comparison was used to compare significant differences between different groups of data. The comparison of results the moisture content were analysed by two-way ANOVA followed by Bonferroni's post-test to compare significant differences between the techniques. A P value of ≤ 0.05 was considered to represent a statistically significant difference.

Chapter 4 - Results and Discussion

4.1. Alginate characterization

The *in vitro* cell culture models are usually formed on 2D surface, however a 3D matrix better mimics the physiological environment by modelling epithelial cells biochemistry and morphology [1]. Therefore, natural polymers such alginate are increasingly being used as a model system for mammalian cell culture due to their chemical versatility and biological performance [5].

The physio-chemical properties of alginate such as swelling ratio, mesh size, mechanical properties can be controlled through different parameters and different studies have demonstrated that this properties can influence on viability, morphology, differentiation and proliferation of cells in crosslinked polymers [54,59,63,64].

Therefore, it is relevant to study the physio-chemical properties of different sodium alginates in order to select the better alginate and gelation conditions that well recreate the mechanical properties found on natural intestinal scenario.

4.1.1. Moisture Content

The determination of moisture content is of extreme importance to estimate the effective alginate concentration (C_{eff}) during the preparation of the alginate gels, rather than considering just the nominal alginate concentration (C_{non}).

The moisture content was obtained by using two different methods. The freeze-drying process can be used for efficient drying but the conditions necessary for preparing and freezing the sample and subsequently perform the freeze-drying process are rigorous which can effect overall technique. Thus, for comparison, infrared radiation was also performed as an alternative technique.

Analyzing the **Figure 17**, the values of moisture content determined by both techniques, in generally, is not statistically significant and demonstrated that the calculated amount of moisture present in the samples is independent of the technique used. Therefore both methods can be used to determine the moisture content of the alginate.

Figure 17 also shows that although the freeze-drying technique presents slightly lower values than those of the infrared radiation technique, all alginates actually have a high moisture content. This result, can be a consequence of the storage conditions along the years. Alginate is a polymer with a hygroscopic behavior. The equilibrium moisture content depends on the amount of water contained in the relative humidity. Thus, the storage conditions is an essential aspect to preserve the stability of sodium alginate [51].

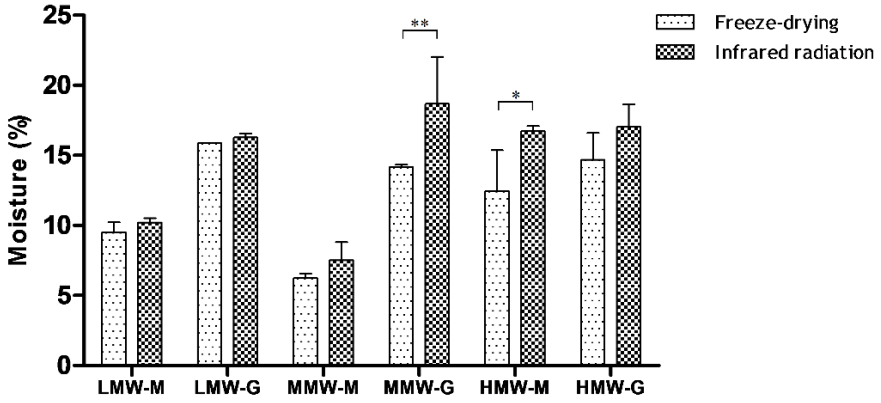

Figure 17 - Moisture content present in each alginate, by freeze-drying and infrared radiation techniques. Results are the average of replicates and bars represent the standard deviation (n=3). The statistical difference between the techniques ($p<0.05$) are denoted by (*).

4.1.2. Viscoelastic properties

The effect of different Ca^{2+}/COO^- molar ratio and alginate concentration on mechanical properties of the different types of alginate is illustrated in **Figure 18**.

At 1% of polymer concentration, rheometry measurements could not be obtained for LMW-G hydrogels at any Ca^{2+}/COO^- molar ratios tested and for LMW-G and MMW-M alginates formed with Ca^{2+}/COO^- molar ratio equal 0.288. Regarding 2% and 3% of polymer concentration, rheometry measurements could not be obtained with LMW-G hydrogels formed with Ca^{2+}/COO^- molar ratio equal 0.288. The integrity of such hydrogels was very low, and they completely deteriorated when placed in culture medium. Theoretically the intramolecular covalent bonds of the polymer backbone are stronger than the intermolecular ionic bonds formed during crosslinking of alginate molecules [54]. This accounted for the lower mechanical integrity of hydrogels with lower molecular weight.

Looking at **Figure 18** we also observed an increase in shear modulus with molar ratio and this increase is more apparent for alginate with medium and higher molecular weights. This results shows that the availability of calcium ions to the COO^- groups plays an important role in mechanical properties. It is documented in the literature that increasing the concentration of calcium increases the amount of calcium ions positioned between consecutive guluronic acid residues creating a thicker ''egg-box'' model and the shear modulus and strength increase due to increase of cross-linked density [54,65].

In general, the G-rich alginate hydrogels present a high increase in shear modulus to as the molar ratio increases, while the M-rich hydrogels only show a slight increase in shear modulus. This conclusion is corroborated by previous studies which revealed that G-rich alginate are more sensitive to changes in the ‘‘egg box’’ configuration, amenable to changes in the strength of the alginate gel, whereas alginates M-rich are not so sensitive to such changes [54].

In the last analysis, however, there are some exceptions. A reduction in the shear modulus was observed at a molar ratio of 0.75 for the 3% MMW-M alginate and for the HMW-G alginate for both concentrations. According to Simpson *et al*. [65] and as also described by Kuo *et al*. [54], a higher Ca^{2+} availability have an influence in gel setting time and the gels exhibit a decrease gelation time rate with the increase of polymer concentration. Possibly, when the gel precursor solution is pipetted some already formed cross-linkes might be destroyed, and heterogeneous hydrogels are formed resulting in the observed reduction of shear modulus.

Kuo *et al*. [54] also reported that shear modulus increases with alginate concentration, because of the higher polymer chain density and entanglement that induce an improvement in mechanical properties. As shown in **Figure 18,** the same results obtained, shear modulus a 3% of concentration is higher than the shear modulus a 2% of concentration, and this is higher than the shear modulus a 1% of concentration.

The relationship between storage (elastic) modulus (G′) and loss modulus (G″) reflect the change of viscosity and elasticity between a weak hydrogel and strong hydrogel. When the G' is higher than the G", the hydrogel present a more elastic-like behavior otherwise it behaves as a viscous liquid [66]. **Figure 18** shows all hydrogels present a G' higher than G", indicating that the elastic behavior of all hydrogels predominates over its viscous behavior and this way exhibit a mechanical elasticity.

The analysis also focused on the differences between the various types of alginate alginates within the same molar ratio. As already stated, and as showed by the data presented in **Table 1**, the different types of alginate tested can be subdivided according to their molecular weight (low, medium or high molecular weight), and their composition, rich in guluronic or guluronic acid. Comparing alginates within each molecular weight group, it is observed, for all concentrations, that the G’ of rich-G alginates are higher than the rich-M alginate. This result is expected, once the intermolecular ionic bonds formed during crosslinking are between consecutive G residues [36]. Therefore the density of cross-linked is higher in alginate with higher guluronic acid content.

It is important to note that the determination of the mechanical properties of each alginate, took into account the conditions that the hydrogels will be subjected during the development of the cellular model. The rheological tests were performed at 37 °C in a humid atmosphere and before the rheology tests, the hydrogel disks were placed in contact with culture medium in order to stabilize their properties. In fact, the hydrogels have the ability to absorb a large amount of water due to its hydrophilic groups, yet still remaining insoluble [67]. As described by several authors, for increased swelling capacity is expected strength of the swollen gels. Thus the behavior of alginates in contact with the medium is described in their properties in order to predict their future behavior for the cell growing.

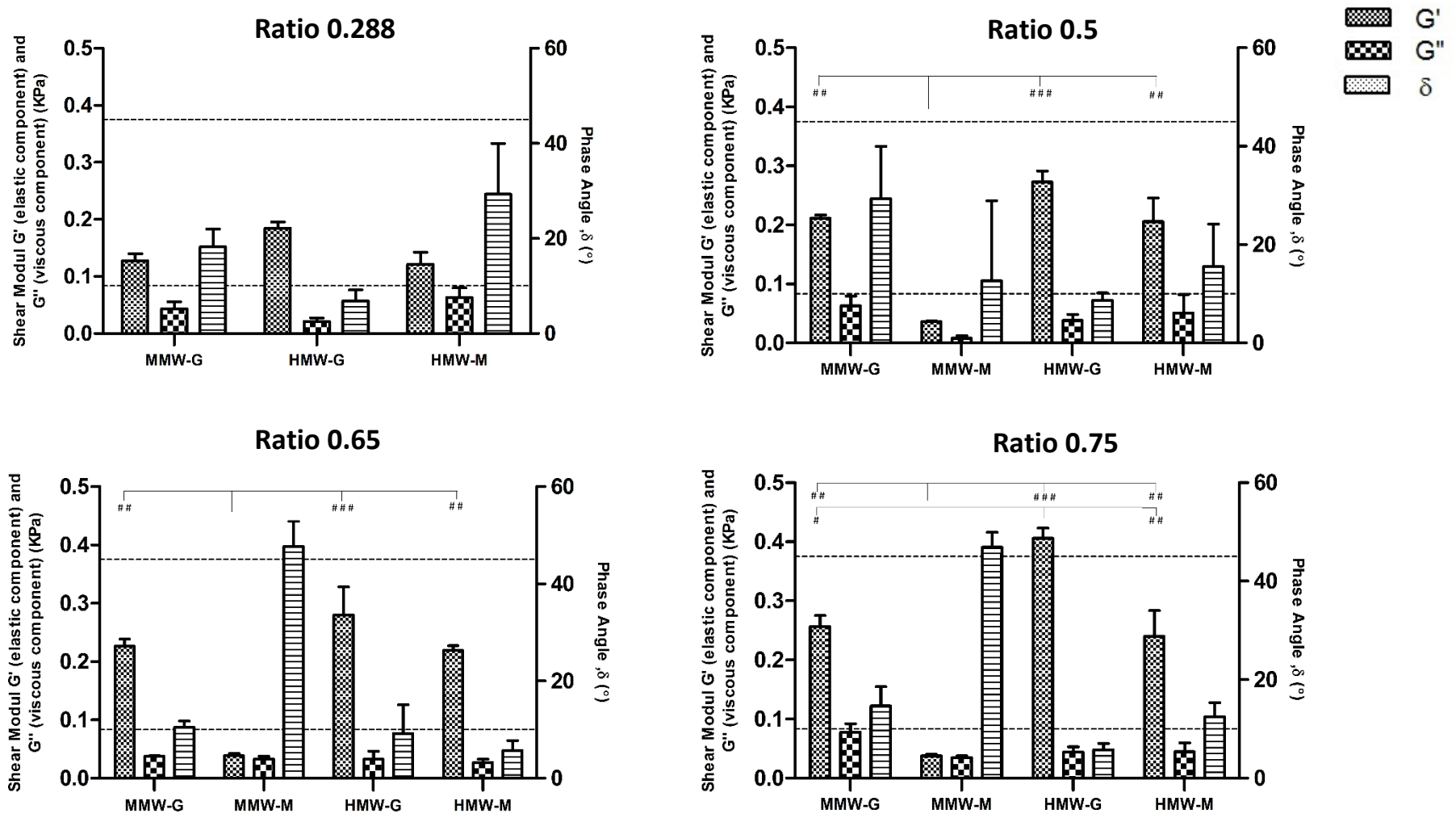

Figure 18.1 – The effect of different Ca^{2+}/COO^- molar ratio on mechanical properties of each alginate, at 1% polymer concentration. Results are the average of replicates and bars represent the standard deviation (n=3). (#) and (*) denotes a significant difference ($p<0.05$), between elastic components and viscous components, respectively.

2% Polymer concentration

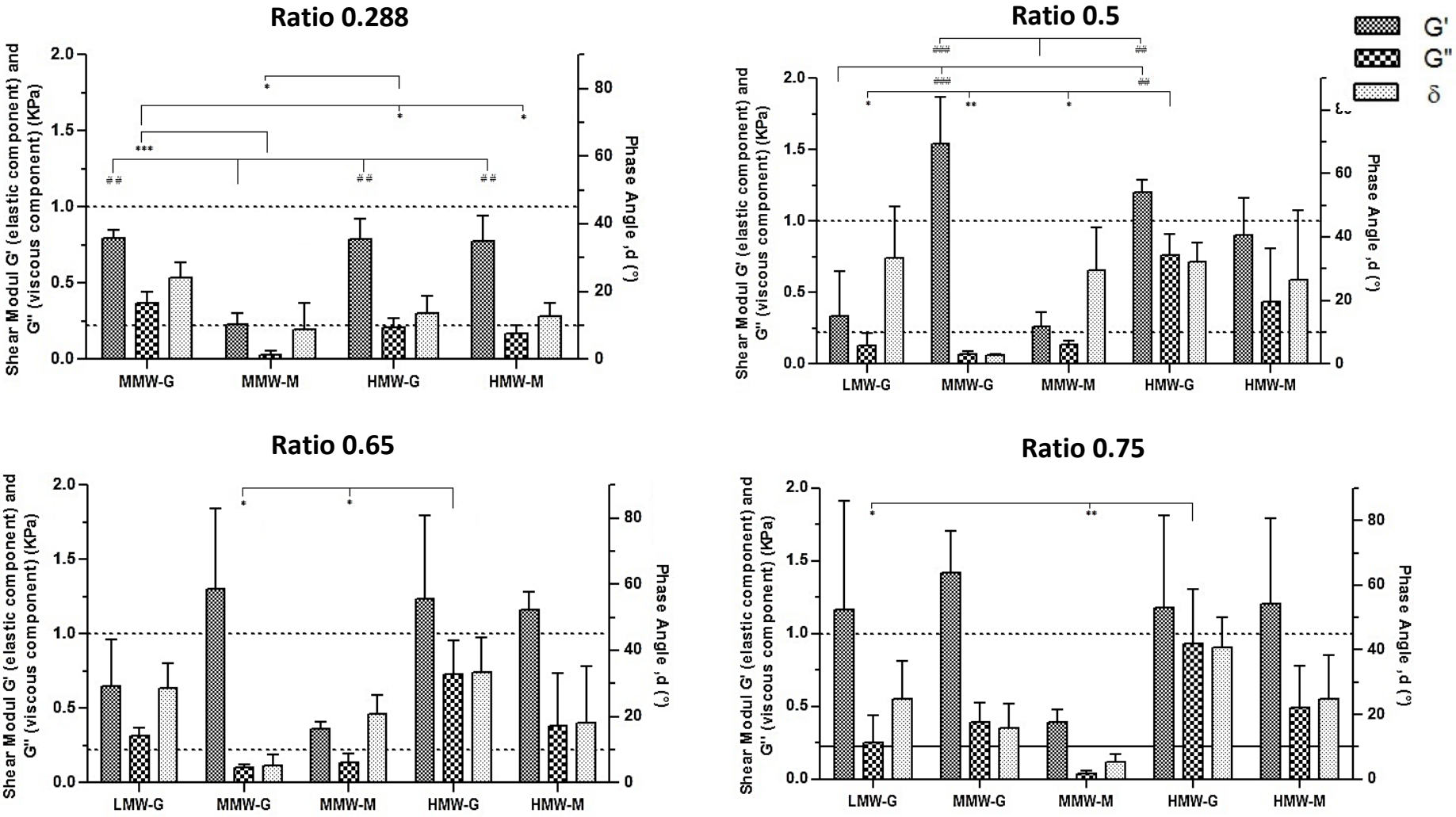

Figure 18.2 - The effect of different Ca^{2+}/COO^- molar ratio on mechanical properties of each alginate, at 2% polymer concentration. Results are the average of replicates and bars represent the standard deviation (n=3). (#) and (*) denotes a significant difference ($p<0.05$), between elastic components and viscous components, respectively.

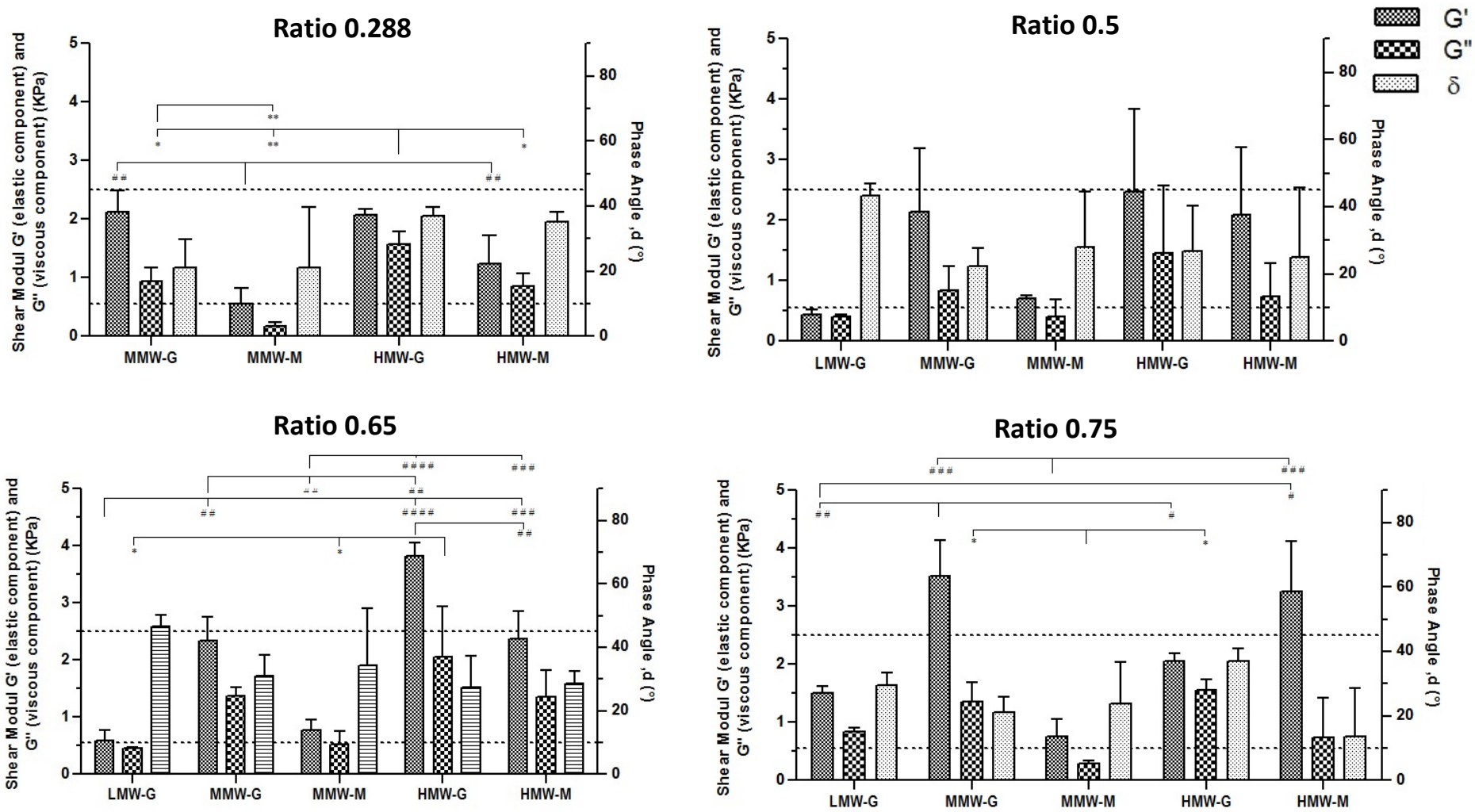

Figure 18.3 - The effect of different Ca^{2+}/COO^- molar ratio on mechanical properties of each alginate, at 3% polymer concentration. Results are the average of replicates and bars represent the standard deviation (n=3). (#) and (*) denotes a significant difference ($p<0.05$), between elastic components and viscous components, respectively.

4.1.3. Swelling ratio

The experiments were conducted to study the effect of the type and sodium alginate concentration on the swelling ratio of alginate hydrogel. The swelling event is consequence of interaction between a solvent and the hydrogel matrix, and express the affinity and exchange of enthalpy between the two forces (free energy and polymer chains) [68].

The results in **Table 3** show that the swelling ratio decreases as the polymer concentration increases and is higher on alginate M-rich. This is due to the fact that the swelling ratio is related to the crosslink density [63]. Swelling degree is defined as the change of dimension of hydrogel matrix. In a crosslinked matrix, the polymer chains begin to elongate under the swelling action of the solvent and this way a stronger hydrogel generate a higher elastic retractive force in opposition to swelling deformation [68]. As we see in rheology results, an increase of alginate concentration induces an improvement in mechanical properties and, therefore, it is expected that highly cross-linked polymer shows less degree of swelling ratio [69].

Following the same thought, alginates M-rich are not so sensitive to changes in the "egg-box", that resulting in less intermolecular ionic bonds and lower values of elastic modulus.

Table 3 – Swelling ration of each type of alginate hydrogel. Results are the mean of three replicates and (±) represent the standard derivations (n=3, mean ± SD).

Alginate type	Swelling ratio, q_F		
	1%	2%	3%
LMW-M	--	--	--
LMW-G	--	35.7 ± 5.0	30.0 ± 1.9
MMW-M	47.4 ± 5.0	35.3 ± 1.1	33.9 ± 1.2
MMW-G	42.5 ± 3.0	33.4 ± 1.2	28.4 ± 1.7
HMW-M	47.7 ± 6.4	44.9 ± 6.1	31.5 ± 6.1
HMW-G	42.7 ± 3.5	37.8 ± 2.4	29.4 ± 1.6

Having regard to the general analysis of rheology and swelling ratio of the six alginates only two alginates will be used in future work.

One of the main functions of the extracellular matrix is to support the tissues, thereby mechanical integrity of a 3D matrix structure is required. Alginates that have a more elastic behavior are ideal for this role. However, the cells are mechanosensitive and a high stiffness

of the matrix acts as a barrier for cells cultured within the matrix [70]. The more dense is the matrix surrounding the cells, the higher the storage modulus, and it becomes more difficult for fibroblasts create sufficient space to spread out, proliferate and migrate [71].

Another point taken into account is the viscosity. As described by Kong, H. and collaborators, a high viscosity solution may not be desirable in terms of maintaining cell viability during the process of hydrogel formation. The cells are exposed to high shear forces during the process and their viability may be compromised [72].

Therefore, and also taking into account some preliminary tests on Transwell® system, HMW-M and HMW-G alginate, at a concentration of 1% and molar ratio of 0.5 were chosen to proceed the work with cell cultures.

The porosity of the hydrogel matrix is a key parameter in the design of artificial ECMs and an important feature for modulating cell behavior. So, we decided to start the cell culture studies first with HMW-M (larger pores) and then with HMW-G (smaller pores) to demonstrated the effect of this parameter in our model, which will be used to mimic intestinal mucosa's architecture and functioning and predict the permeability of a model drug.

4.1.4 Characterization of RGD-Alginate

Alginate is inherently a non cell-interactive polymer, composed of monomers lacking appropriate ligands that are crucial to promote and regulate cell interaction. One of the strategy to fit this drawback is covalently modifying alginate introducing adhesion peptide, such RGD, as side-chains, using sing aqueous carbodiimide chemistry [40]. The N-terminal of the peptide is linked to the carboxylic groups along the alginate polymer chain [58].

Therefore, HMW-M alginate was chemical modified with 16.7 mg of cell-adhesion RGD peptide and the coupling efficiency was 70.7%. Therefore, in 1000mg of alginate are 11.8 mg of RGD.

Knowing that in a gram of alginate have:

$$\mathrm{N_{monomers}} = \frac{\text{mass of alginate}}{\mathrm{M}_R} = \frac{1}{198} = 5.05 \times 10^{-3} \text{moles of monomers},$$

where $N_{monomers}$ is the moles of monomers present in alginate and M_R is the monomer molecular weight,

Since each monomer have a carboxylic acid group then a gram of alginate have 5.68×10^{-3} mole of carboxyl groups. This way per gram of HMW-M alginate we have 5.96×10^{-5} mole of carboxyl groups with RGD.

Other important data is the amount of RGD present in hydrogel. If the final concentration of hydrogel is 1% (w/v):

$$[\mathrm{M}_{RGD}] = \frac{\text{mass of RGD in Hydrogel}}{\mathrm{M}_{RGD}} = \frac{0.118}{758.74} = 155.6 \text{ μM of RGD in Hydrogel at 1\% (w/v)},$$

where MRGD is the RGD molecular weight of guluronic (758.74 g.mol-1).

To evaluate the barrier integrity of epithelium cells, we used other alginate M-rich, the PRONOVA UPLVM. Regarding this alginate, the chemical modification was performed with 100 mg of RGD peptide and the coupling efficiency was 20.5%. Therefore, in in 1000 mg of alginate we have 20.49 mg. Following the same principle above describe, per gram of UPLVM alginate we have 1.03×10^{-4} mole of carboxyl groups with RGD and the amount of RGD present in hydrogel at 1% (w/v) is 270.1 μM.

4.2. Cell culture studies

4.2.1. Analysis of CCD18-Co cells under 3D behaviour

In vivo, intestinal myofibroblasts (IMFs), also called pericryptal fibroblasts, reside subjacent to the basal membrane and are able to secrete matrix molecules that impart unique characteristics to lamina propria, cell surface and the ECM of small intestinal [73]. In order to mimic this environment, our intestinal *in vitro* model comprise IMFs (CCD18-Co cells) embedded in alginate hydrogel. This configuration was adopted taking into account our previous work [61].

4.2.1.1. Effect of cell density on myofibroblast viability and metabolic activity in 3D

The experiment was conducted to investigate the effect of cell density on CCD18-Co cells viability and metabolic activity under 3D conditions. Results of the metabolic activity assays are presented in **Figure 19,** while the results related with CCD18-Co cells viability are present in **Figure 20.** Controls were used in the experiment, namely alginate without RGD under the same conditions. This was conducted also to evaluate the effect of the presence of RGD peptide in viability and metabolic activity of CCD18-Co cells.

It can be seen from the **Figure 19** that metabolic activity of the CCD18-co cells had a significant decrease over 21 days of culture in both types of hydrogel matrices. After 4 days, cells within hydrogel matrices present a higher viability compared to other culture time. After 7 days, the metabolic activity decreases nearly halved and it is more pronounced for the cells within RGD-alginate hydrogel at density D2 ($5X10^6$ cells/mL).

In vitro cultures and under 3D conditions may require a dynamic environment enabling a constant perfusion of nutrients, as the hydrogel matrix may lead to some hypoxia. The hydrogel may also provide a physical obstacle to cell proliferation, leading to growth arrest [74,70]. These processes are more likely to occur in high densities, which can probably explain the remarkable difference that between density D2 ($5X10^6$ cells/mL) and D1 ($1X10^6$ cells/mL) in unmodified hydrogel, as shown in **Figure 19|A.**

When cells were embedding in RGD-alginate hydrogel differences between D1 and D2 became less apparent. As we describe before, similarly to other hydrophilic polymers, the alginate is a non-cell-adhesive, for that reason it is expected that modified alginate can

promote cell-matrix interactions and improve cell function and responses, namely under more hostile conditions [5]. Then, as depicted in **Figure 19|B,** the CCD18-Co cells at density D2 present a better metabolic activity in alginate with RGD.

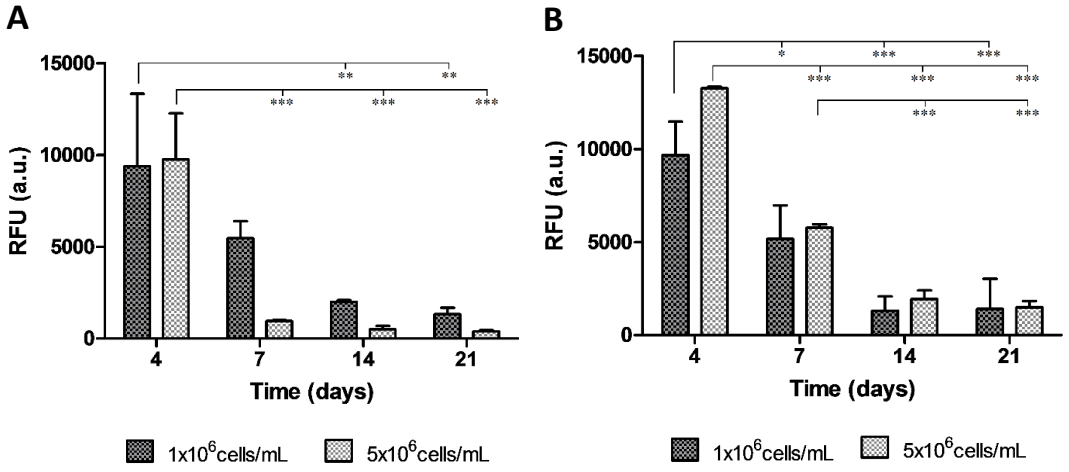

Figure 19 - Metabolic activity of CCD18-Co cells cultured in 3D along 21 days at different densities: A| Metabolic activity of CCD18-Co within unmodified alginate hydrogel; **B|** Metabolic activity of CCD18-Co within RGD- alginate hydrogel. Results are the average of replicates and bars represent the standard deviation (n=3). The statistical difference between the techniques ($p<0.05$) are denoted by (*).

In conjunction with metabolic activity studies, live/dead assay images were also obtained to qualitatively indicate the viability of the CCD18-Co cells with alginate hydrogel at day 21.

As shown in **Figure 20|B** and **Figure 20D,** CCD18-Co cells at density D2 present higher viability in RGD-alginate compared to unmodified alginate. This probably indicate that density D2 is effected by presence of RGD peptide in hydrogel matrices to maintain the cell function and consequently their viability under 3D conditions.

Regarding to density D1, as shown in **Figure 20|A** and **Figure 20|C**, the presence of RGD peptide did not have grate influence in cell viability. With this density, nutrient diffusion and proliferation limitation associated to higher density cultures were probably irrelevant and therefore did not affected cellular viability. Overall, the result of cell viability are in agreement with the metabolic activity results as we expected.

Different studies have been shown that an increasing of the cell density affect distinctively the cellular activities, such as protein production and as cluster formation [75,60]. Therefore, taking into account to the general analysis of viability and metabolic activity results and also from the literature, density D2 ($5X10^6$ cells/mL) indicated to be an optical density to adopt on the following experiments and on tridimensional *in vitro* model.

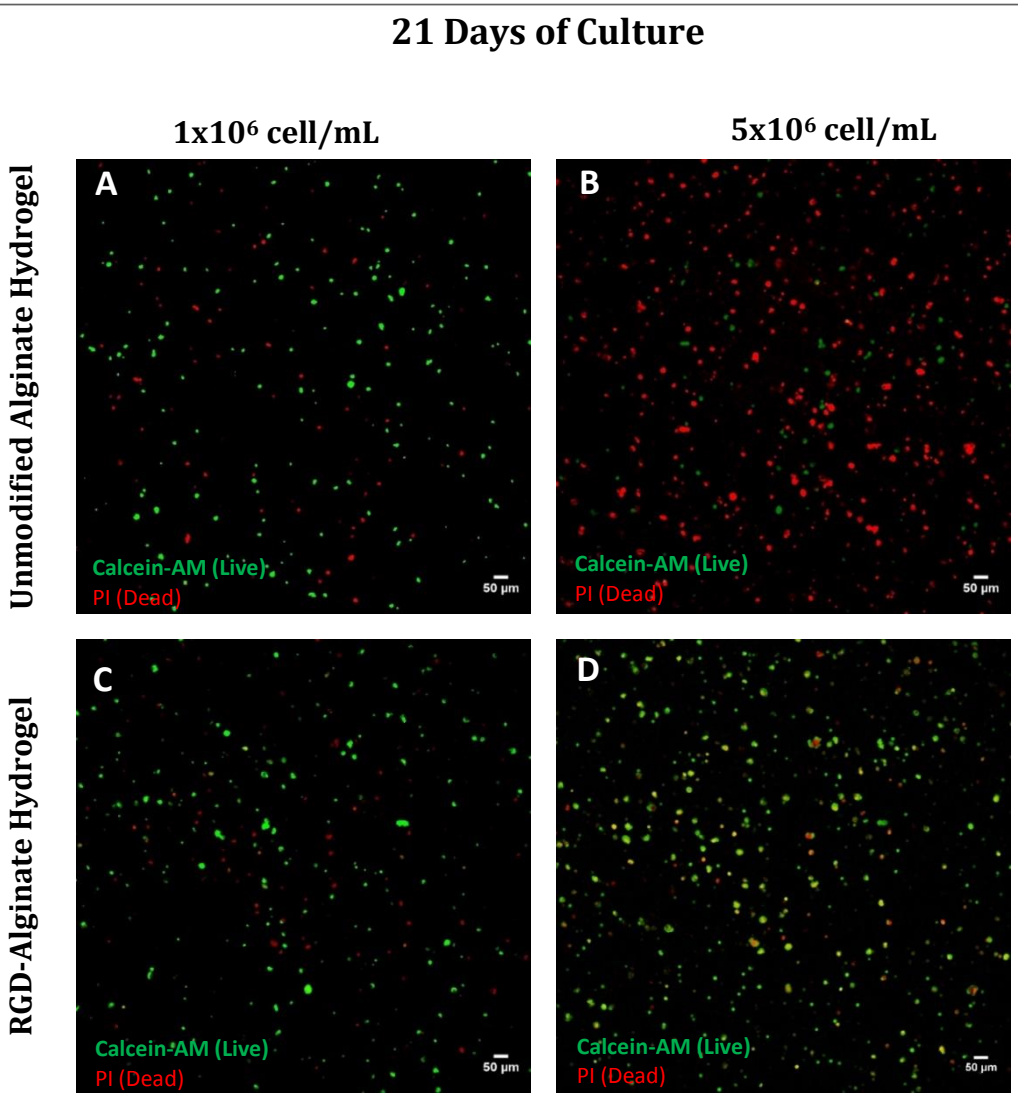

Figure 20 – Live/Dead viability assay performed in CCD18-Co cells cultured under 3D conditions within alginate hydrogel with or without RGD peptides 21 days after culture at different densities. A-B| Cell viability of CCD18-Co cells grown on unmodified alginate for two different cell densities (D1=1x10^{6}cell/mL and D2=5x10^{6}cell/mL); **C-D|** Cell viability of CCD18-Co cells grown on RGD-alginate hydrogel for two different cell densities (D1=1x10^{6}cell/mL and D2=5x10^{6}cell/mL). Live cells are stained in green (calcein-AM) and dead cells are stained in red (PI). Scale bar 50µm.

4.2.1.2. Cell morphology

To investigate the morphology of CCD18-Co cells and their spatial arrangement in 3D conditions, H&E (**Figure 21|A**) and Vimentin (**Figure 21|B**) stainings were performed.

After 21 days of culture, in both experiments, CCD18-Co cells within RGD-alginate hydrogel adopted a spherical shape and were homogeneously distributed through the matrix. This morphology was already observed in previous studies. For example, Hakkinen, K. *et al*. [76] showed that human foreskin fibroblasts, in 3D environment, were more spindle shaped with a fewer lateral protrusions than on 2D conditions. Also Cunha *et al*. [77] showed that stiffness of the surrounding biomaterial extremely effected the morphology of fibroblast. Cells probed the

mechanical properties of their adhesion substrate, and also dynamically reorganized their cytoskeleton in response to the resistance that they detected. So, cells spread extensively in soft substrates, but presented a spherical shape in higher stiffness matrix. After a certain crosslinking density, because of the increased resistance to deformation of the matrix, cells were no longer able to spread inside this matrices [59].

The adhesion between cells and the ECM involve receptor binding but also physical interactions, in other words, the mechanical forces also play a role in numerous adhesion events [78]. Therefore, there are three major classes of microenvironments factors that can be influence the cellular behaviour and subsequent the morphology of cells on different conditions: the biomechanical composition of matrix, the physical parameters of the matrix and the special cues [79,80] .

Regarding the presence of RGD binding sites, it has been previously demonstrated by others that although the matrix might present increasing numbers of binding sites to which fibroblast can adhere, fibroblast can still fail to spread, suggesting that cell morphology is not affected only by the availability of adhesion sites [59].

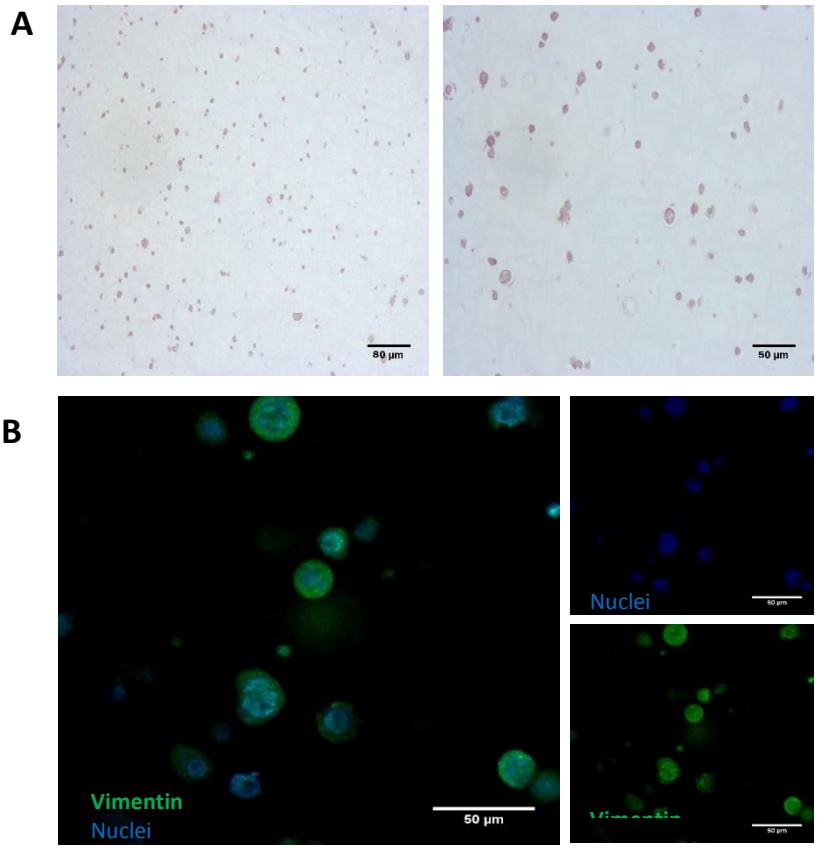

Figure 21 – Intestinal myofibroblast morphology cultured under 3D conditions at 21days. A| H&E stained paraffin section showing CCD18-Co-laden hydrogel at 21 days of culture. H&E stains cells in dark/purple. Scale bar 80µm and 50µm. **B|** Vimentin are labelled with AlexaFluor 488 (green) and nucleus with DAPI (blue). Scale bar 50µm.

4.2.1.3. ECM components

IMFs are able to secrete collagen and various matrix proteins, such as fibronectin (FN), that are important to remodel the ECM and are components that interact specifically with different cells and promote the cell adhesion [73,81]. In order to investigate the deposition of this ECM components (FN and collagen) in 3D conditions, picrosirius red (**Figure 22|A**) and FN (**Figure 22|B**) stainings were performed.

Booth results demonstrate CCD18-Co cells played a role in the remodeling of the surrounding hydrogel network, which substituted to some extent by CCD18-Co self-produced components. However, FN and collagen expression were detected essential intracellularly and assembled on the pericellular space. This fact, can be partially explained by the lack of cell aggregation inside the hydrogels. Maia *et al.*[60] shown that the formation of mesenchymal stem cell aggregates was related with the local deposition of the fibronectin and this aggregation was only detected for initial densities above $15x10^6$ cell/mL. Also Robinson *et al.*[82] demonstrated that in cell aggregates occur cell-FN-cell interactions that can generate sufficient tension to support FN fibril assembly in the absence of both FN-substrate and cell-substrate adhesion. Remarkably, cell aggregation was shown to result in enhanced endogenous ECM production.

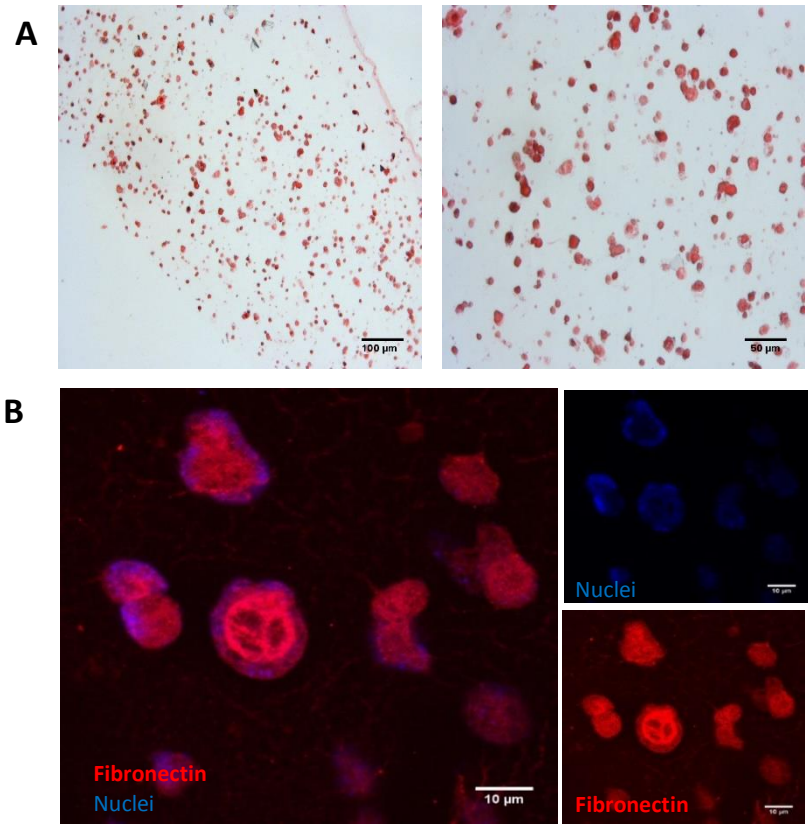

Figure 22 – ECM components of Intestinal myofibroblast cultured under 3D conditions at 21days. A| Picrosirius red stained paraffin section of CCD18-Co-laden hydrogel at 21 days of culture. Picrosirius red stains collagen in red. Scale bar 100µm and 50µm. **B|** Fibronectin are labelled with AlexaFluor 594 (red) and nucleus with DAPI (blue). Scale bar 10µm.

4.2.2. Intestinal models

The studies previously described were aimed to establish the bottom line of the 3D model that resembles the native mucosa. In the following studies, the hydrogel with CCD18-Co was used the support the epithelium cells, similarly to the native small intestinal mucosa in which the epithelium cells layer over lamina propria.

4.2.2.1. Evaluating barrier integrity

A characteristic feature of human intestinal epithelium is the monolayer tightness. The epithelial barrier function is regulated by the apical intercellular junction, denominated as the tight junction (TJ). These junctions resulting in a protected barrier that are key to prevent paracellular diffusion [12]. An intact monolayer it than crucial to the biological process and the integrity and maturity of the monolayer can be quantitatively measured through the transepithelial electric resistance (TEER), where higher values represent an increase of the monolayer integrity.

To investigate the integrity of monolayer in 3Dl *in vitro* intestinal model, we started by studying the integrity of $C2_{BBe}1$ monolayer in hydrogel without myofibroblast (HMW-M/ $C2_{BBe}1$ model).

The initial density of $C2_{BBe}1$ used was $1X10^5$cells/cm^2, as previously optimized [4]. However, when using this density in hydrogel with 155µM, cells were not able to form a monolayer, as we can observe in **Figure 23|A** and qualitatively in **Figure 24|A.**

This way, in order to increase the monolayer integrity, we decided to increase the amount of RGD peptide in hydrogel matrix (155µM, 200µ and 300µM) with the aim improving the cell adhesion between epithelial cells and hydrogel. However, as depicted in **Figure 23|A,** this improvement was not enough to epithelium cells formed a tightness monolayer.

The next step was to try other alginate hydrogel formulations, namely UPLVM (similar to HMW-M, with 155µM of RGD) and also different gelation process, namely external gelation. As observed in **Figure 23|B,** the lack of formation of an integrity monolayer was not depended/influence by the type of alginate and the gelation nature.

The following experiments consisted in increasing the density of the epithelial cells (D1=$1X10^5$cells/cm^2, D2=$2X10^5$cells/cm^2 and D3=$4X10^5$cells/cm^2) in both types of hydrogel.

In **Figure 23|B** and **Figure 24|B**, it is possible to visualize that HMW-M hydrogel with an initial density D3, had an improvement in monolayer integrity. Focusing on this density and hydrogel, we decided to improve some culture conditions. Initial, the $C2_{BBe}1$ monolayer was prepared by seeding $C2_{BBe}1$ at a density D3 on volume of 500µL but later, to prevent adherence of some of the epithelium cells to the wall of the Transwell (that was observed on previous experiments), the $C2_{BBe}1$ monolayer was prepared by seeding $C2_{BBe}1$ at a density D3 on lower volume (80µL). The culture medium volume was only completed after an adhesion period (2.5 hours), as the cell adhesion process involves two important phases. During the first phase, cells attach to the substrate involving an interaction between cell surface receptors and specific ligands on the substrate. This event occurs over a short time period. A second phase is cell

spreading that begins after the initial contact and continuous during and after first hour of cell attachment [83,84].

As demonstrated in **Figure 23|C,** the TEER continuously increased during the 21 days of culture. Although the Caco-2 cells are characterized by TEER values comprised between 150-1600 Ω.cm^2, presenting values demonstrate the HMW-M/C2$_{BBe}$1 model start to present a required integrity and confluent membrane [22]. In fact, Carla et al. also shown a significant lower TEER value over the 21 days between CCD18-CO+Matrigel/Caco-2 model and Caco-2 cell model. The behavior of epithelium cells is modulated by the type of culture substrate, and when C2$_{BBe}$1 cells are grown on matrices like hydrogel and matrigel membrane integrity is affected. When analyzing the control C2$_{BBe}$1 model, as depicted in **Figure 25**, we can see that in this case the model reached a desirable integrity above 300 Ω.cm^2.

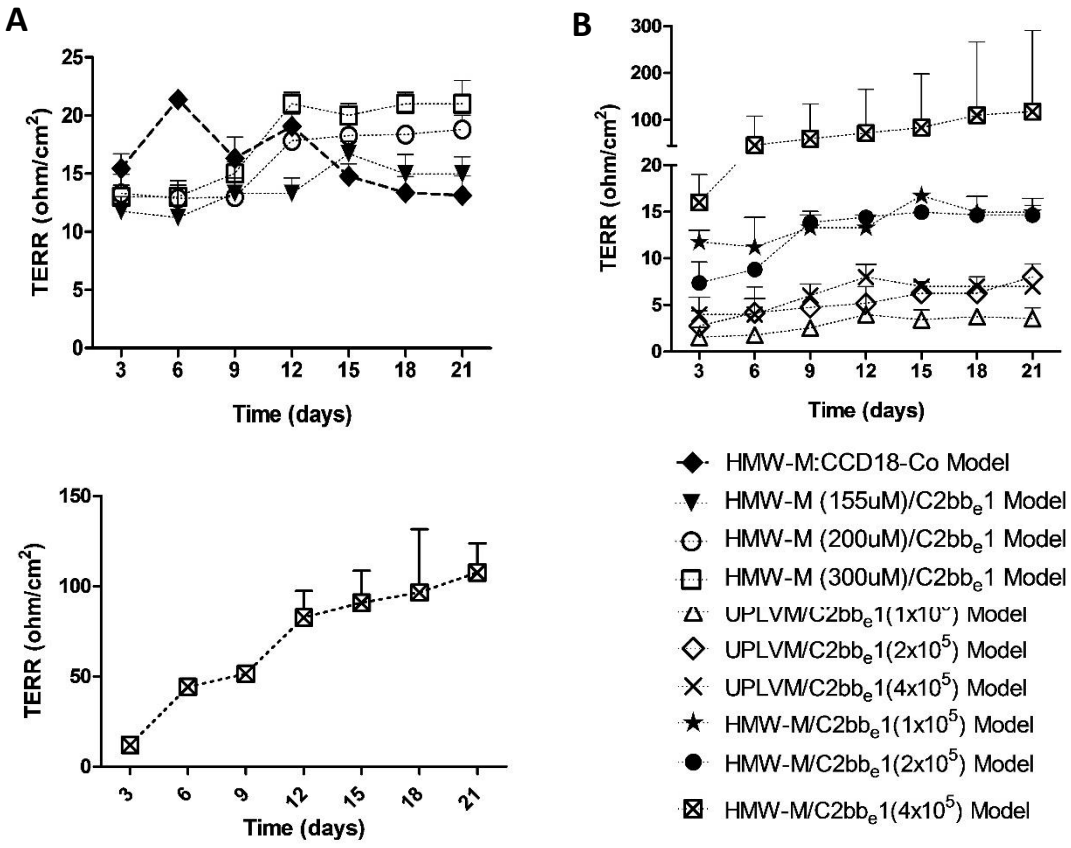

Figure 23 - TEER cell measurement monitored in function of time during the 21 days of culture comprising CCD18-Co and C2$_{BBe}$1 cells. Results are the average of replicates and bars represent the standard deviation (n=3).

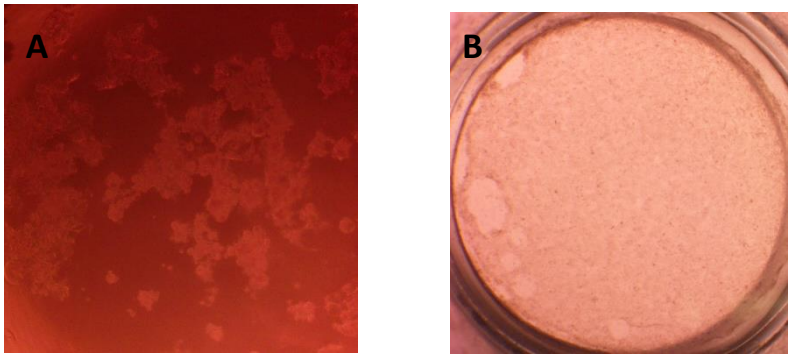

Figure 24 – Microscope loupe images of HMW-M/C2$_{BBe}$1 model at 21 days of culture with different initial densities. A| HMW-M/C2$_{BBe}$1 model with a C2$_{BBe}$1 initial density of 1X10^{5}cells/cm^2, **B|** HMW-M/C2$_{BBe}$1 model with a C2$_{BBe}$1 initial density of 4X10^{5}cells/cm^2.

As control, C2$_{BBe}$1, C2$_{BBe}$1/HT29-MTX and C2$_{BBe}$1/HT29-MTX/Raji B models were performed. Overall the membranes present an increase along with the culture and a monolayer integrity, however due the different morphologies of the cells, it was expected TEER values measurement being highest in C2$_{BBe}$1 model and lowest in the triple co-culture, as depicted in **Figure 25**.

As described by Hilgendorf *et al*. [85] the Caco-2 monolayer display higher TEER values due the fact that TJ are very tight between enterocytes.

When comparing C2$_{BBe}$1 cell model to the C2$_{BBe}$1/HT29-MTX co-culture, there seems to be similar growth but due the presence of mucus-secreting HT29-MTX, the co-culture model values lower than those of monolayer [85].

Looking at the triple co-culture model, it was expected that the TEER values presented similar values to the C2$_{BBe}$1/HT29-MTX co-culture since this model is comprised mostly by C2$_{BBe}$1 and HT29-MTX cells. However, the TEER values obtained were lower, probably due the conversion of C2$_{BBe}$1 epithelial cells into M-like cells by introduction of Raji B lymphocytes (day 15), and the TJs rearrangement between enterocytes and M-like cells are not so tight as the C2$_{BBe}$1/HT29-MTX co-culture. This evidence was already reported by Araújo *et al*. [4].

In the future, when establish the tridimensional co-culture models: Hydrogel+CCD18-Co/ C2$_{BBe}$1/HT29-MTX and Hydrogel+CCD18-Co/ C2$_{BBe}$1/HT29-MTX/Raji B, will be expected the same TERR profile between models.

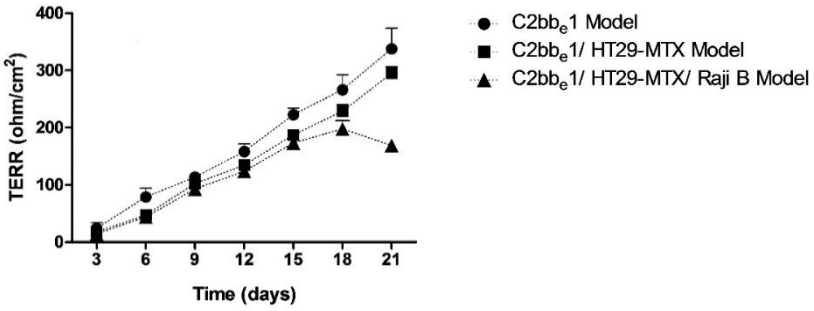

Figure 25 - TEER cell measurement monitored in function of time during the 21 days of culture comprising C2$_{BBe}$1, HT29-MTX and Raji B cells. Results are the average of replicates and bars represent the standard deviation (n=3).

4.2.2.2. Insulin permeability

After establishment of a tridimensional C2BBe1 model, insulin transport studies was conducted to analyses the functional character of the model through comparison the permeability profile of insulin in the C2BBe1 monolayer.

At different time points, TEER was measure to evaluate the integrity of $C2_{BBe}1$ monolayer along the permeability assay. As depicted in **Figure 26|A,** the two models showed the same profile in TEER measurement. During the first hour, the TEER values decreased in both models with a more pronounced decrease in the $C2_{BBe}1$ model.

Due the high hydrophilicity of insulin, the paracellular pathway is the real contribution of insulin across the intestinal epithelium [86]. This way, the initial decreased of TEER values can be explained to the fact the insulin compounds interact with cell layer, resulting in the opening of Tjs to promote the paracellular transport of insulin.

As observed in **Figure 26|B,** the permeability profile follows the same tendency, were the increase of permeability was related to the decrease the TEER values. The hydrogel/$C2_{BBe}1$ model present the lower initial TEER values that reflected a lower integrity of the monolayer. Thus, as expected, this model allowed higher permeation to the passage of insulin.

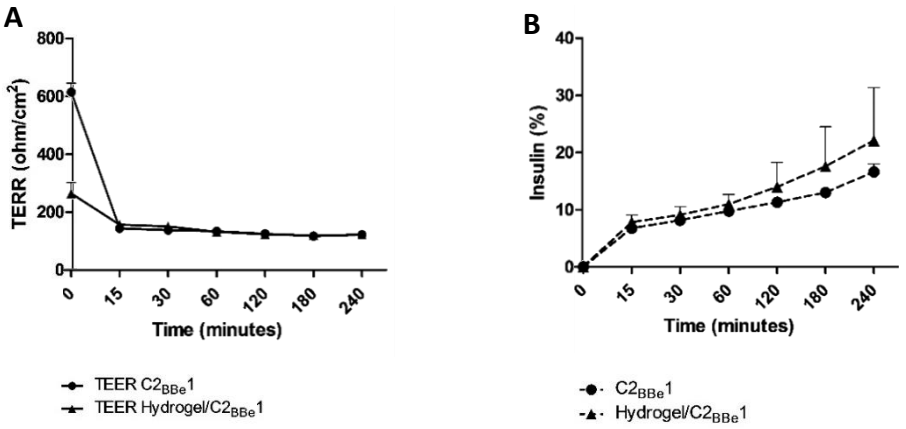

Figure 26 – TEER cell monolayer measurements and cumulative insulin transport across monoculture of $C2_{BBe}1$. A|TEER values of $C2_{BBe}1$ monolayer monitored during 4hours of permeability experiments, **B|** Cumulative insulin transport across monoculture of C2BBe1. Results are the average of replicates and bars represent the standard deviation (n=3).

This observation is also supported by the results of apparent permeability coefficient (P_{aap}), shown in **Table 4.** The P_{aap} represents a cumulative amount of the test compound in the basolateral side. A higher permeability coefficient are correlated with completely absorbed drugs (P_{aap}> 1 $\times 10^{-6}$ cm/s) whereas lower permeability coefficient are correlated with incompletely absorbed drugs (P_{aap}< 1 $\times 10^{-7}$ cm/s) [87].

The P_{aap} value to insulin in $C2_{BBe}1$ model was higher 1×10^{-6} cm/s but, as expected, presented the lower P_{app}. However this difference in P_{aap} values is not statistical significant that suggest the presence of hydrogel layer does seem to create a barrier to the passage of insulin molecules.

Overall, despite the tridimensional model did not present a cohesive membrane compared with the respective monolayer of control, the P_{aap} of insulin is not so affected.

Table 4 – Apparent permeability coefficient P_{aap} ($\times 10^{-6}$ cm/s) of insulin across the $C2_{BBe}1$ and hydrogel/$C2_{BBe}1$ models. Results are the mean of three replicates and (±) represent the standard derivations (n=3, mean ± SD).

In vitro models	P_{aap} ($\times 10^{-6}$ cm/s)	Significant difference
$C2_{BBe}1$	7.66 ± 0.63	ns
Hydrogel/ $C2_{BBe}1$	10.2 ± 4.28	

The results from P_{aap} showed also that tridimensional model was efficient in predicting insulin permeability, as compared to the P_{aap} values of insulin across *ex vivo* rat ileum model, presented in **Table 5.**

Table 5- Apparent permeability coefficient P_{aap} ($\times 10^{-6}$ cm/s) of insulin across *ex vivo* intestinal.

	Rat Ileum [88]	Rat Ileum [89]	Rat Ileum [90]
P_{aap} ($\times 10^{-6}$ cm/s)	0.60 ± 0.02	0.90 ± 0.10	7.35 ± 1.18

4.2.2.3.2. FITC-Dextran permeation

The 4 kDa FITC-Dextran is a fluorescent molecule that able to across the epithelium layer through paracellular pathway being a good way to evaluate the integrity of the membrane [91]. Therefore, after permeability studies, FITC-Dextran permeation was performed.

As depicted in **Table 6,** the rejection of the FITC-Dextran, in other words, the amount of this small molecule which was retained in the apical side was above 75%. This result showed that despite the low values presented in the insulin permeability, the presence of insulin molecules did not disrupted the Tjs and its opening was reversible. In fact, the reversibility of lower TEER values after the permeability studies has been reported by other authors [92].

Table 6 – Permeability of FITC-Dextran across the $C2_{BBe}1$ and hydrogel/$C2_{BBe}1$ models after insulin permeability. Results are the mean of three replicates and (±) represent the standard derivations (n=3, mean ± SD).

In vitro models	Rejection FITC-Dextran (%)	Significant difference
$C2_{BBe}1$	89.74 ± 0.51	ns
Hydrogel/ $C2_{BBe}1$	76.52 ± 11.70	

Chapter 5 - Conclusions

Conclusions e Future Perspectives

This Thesis aims to develop an intestinal tissue engineering model based on intestinal fibroblasts and epithelial cells supported by a natural biomaterial, the alginate.

In order to establish the bottom line of the 3D intestinal *in vitro* model, we started by evaluating physical-chemical characteristics of different type of sodium alginate. Our results showed that the shear modulus increased with alginate concentration, calcium content, molecular weight and guluronic acid content, and also demonstrated that the type and concentration of sodium alginate effected the swelling ratio and mesh size of resulting hydrogels. Therefore, changing different parameters in the formation of alginate hydrogels enables their viscoelastic properties to be modulated to better recreate the properties found on natural intestinal mucosa.

Additionally, we explored the behaviour of CCD18-Co cells in a 3D matrix through cell viability and metabolic activity analyses. The cell density of $5x10^6$ cells/mL showed be the most suitable density to be used over 21 days, which corresponds to the period necessary to fully differentiate $C2_{BBe}1$ cells. Morphologically, the myofibroblasts presented a spherical shape, which was associated to the matrix stiffness and, probably due the lack of cell aggregation, ECM compounds were essentially detected intracellularly and assembled at the pericellular space.

In order to characterize the epithelium layer of intestinal mucosa, the monolayer tightness of the $C2_{BBe}1$ cells was evaluated. The initial density of $4x10^6$ cells/mL was the density that started to present an acceptable integrity and maturity of the monolayer, although still presenting a lower TEER value when compared with $C2_{BBe}1$ model. The hydrogel is a critical factor for the barrier formation, however the tridimensional $C2_{BBe}1$ model showed to be efficient in the predicting of insulin permeability.

Although the ultimate goal was not achieved, results from this thesis will hopefully help to develop, in a future work, an improved 3D in vitro model that closely mimics the intestinal mucosa.

The intestinal model can comprise intestinal fibroblast (CCD18-Co cells) embedded in RGD-alginate solution to a final density of the 5×10^6 cells/mL. Epithelial co-culture of $C2_{BBe}1$ and HT29-MTX cells suspension seeded at final density of 4×10^5cells/cm^2 (90:10 proportion) on

apical side and 0.7×10^5cells/24-well Raji B lymphocytes are seeded on the basolateral side (**Figure 27**).

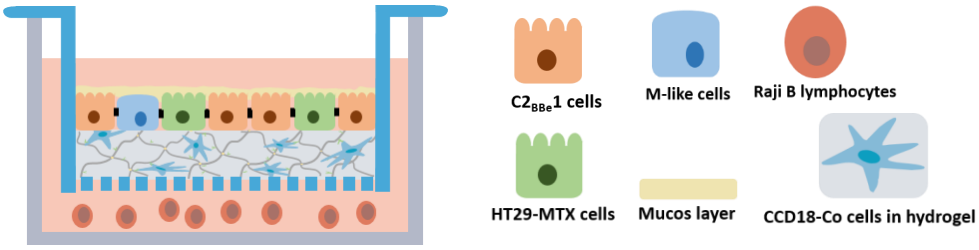

Figure 27 - Schematic illustration of the tridimensional in vitro model: On CCD18-Co-laden hydrogel in a Transwell system, $C2_{BBe}1$ and HT29-MTX cells suspension (9:1) were gently. Raji B cells were added on the basolateral chamber of 14-day of culture and further maintained for 4-6days.

It will be imperative a full characterization of the intestinal tridimensional in vitro model, at a biological and physicochemical level and also test the efficacy of drug absorption mechanisms and increment of robustness and functionality of the tissue engineering model.

Additionally, will be interesting study the ECM with HMW-G alginate to understand the effect of G-rich sodium alginate in intestinal mucosa's architecture and functioning and predicts the permeability of a model drug.

Finally, it will be interesting understand how the presence of HT29-MTX and M cells can influence the $C2_{BBe}1$ cell differentiation and how the initial cell density of Raji B cells affects the amount of M-like cells and further optimized the density of lymphocytes in the intestinal in vitro model.

Chapter 6 - References

[1] C. M. Costello, J. Hongpeng, S. Shaffiey, J. Yu, N. K. Jain, D. Hackam, and J. C. March, "Synthetic small intestinal scaffolds for improved studies of intestinal differentiation.," *Biotechnol. Bioeng.*, vol. 111, no. 6, pp. 1222–32, Jun. 2014.

[2] K. M. Wood, G. M. Stone, and N. A. Peppas, "The effect of complexation hydrogels on insulin transport in intestinal epithelial cell models.," *Acta Biomater.*, vol. 6, no. 1, pp. 48–56, Jan. 2010.

[3] I. M. van der Lubben, F. A. C. van Opdorp, M. R. Hengeveld, J. J. M. Onderwater, H. K. Koerten, J. C. Verhoef, G. Borchard, and H. E. Junginger, "Transport of chitosan microparticles for mucosal vaccine delivery in a human intestinal M-cell model.," *J. Drug Target.*, vol. 10, no. 6, pp. 449–456, Sep. 2002.

[4] F. Antunes, F. Andrade, F. Araújo, D. Ferreira, and B. Sarmento, "Establishment of a triple co-culture in vitro cell models to study intestinal absorption of peptide drugs.," *Eur. J. Pharm. Biopharm.*, vol. 83, no. 3, pp. 427–435, Apr. 2013.

[5] J. Sun and H. Tan, "Alginate-based biomaterials for regenerative medicine applications.," *Materials (Basel).*, vol. 6, no. 4, pp. 1285–1309, Mar. 2013.

[6] P. V Balimane and S. Chong, "Cell culture-based models for intestinal permeability: a critique.," *Drug Discov. Today*, vol. 10, no. 5, pp. 335–43, Mar. 2005.

[7] R. Seeley, T. Stephens, and P. Tate, *Anatomy and physiology.*, 6ª edition. McGraw-Hill, 2003.

[8] Standring and Susan, *Gray's anatomy.*, Fortieth e. London: Elsevier Ltd, 2008, pp. 111–2671.

[9] H. Clevers, "The intestinal crypt, a prototype stem cell compartment.," *Cell*, vol. 154, no. 2, pp. 274–84, Jul. 2013.

[10] N. Barker, "Adult intestinal stem cells: critical drivers of epithelial homeostasis and regeneration.," *Nat. Rev. Mol. Cell Biol.*, vol. 15, no. 1, pp. 19–33, Jan. 2014.

[11] P. Simon-Assmann, N. Turck, M. Sidhoum-Jenny, G. Gradwohl, and M. Kedinger, "In vitro models of intestinal epithelial cell differentiation.," *Cell Biol. Toxicol.*, vol. 23, no. 4, pp. 241–56, Jul. 2007.

[12] T. Kucharzik, S. V Walsh, J. Chen, C. A. Parkos, and A. Nusrat, "Neutrophil transmigration in inflammatory bowel disease is associated with differential expression of epithelial intercellular junction proteins," *Am. J. Pathol.*, vol. 159, no. 6, pp. 2001–2009, 2009.

[13] C. S. Lee and K. H. Kaestner, "Clinical endocrinology and metabolism. Development of gut endocrine cells.," *Best Pract. Res. Clin. Endocrinol. Metab.*, vol. 18, no. 4, pp. 453–462, Dec. 2004.

[14] G. Rindi, A. B. Leiter, A. S. Kopin, C. Bordi, and E. Solcia, "The 'normal' endocrine cell of the gut: changing concepts and new evidences.," *Ann. N. Y. Acad. Sci.*, vol. 1014, pp. 1–12, Apr. 2004.

[15] T. Kanaya, H. Aso, K. Miyazawa, T. Kido, T. Minashima, K. Watanabe, S. Ohwada, H. Kitazawa, M. T. Rose, and T. Yamaguchi, "Staining patterns for actin and villin distinguish M cells in bovine follicle-associated epithelium.," *Res. Vet. Sci.*, vol. 82, no. 2, pp. 141–149, Apr. 2007.

[16] M. Russell, "Mucosal Immunity," in *New Bacterial Vaccines SE - 5*, Springer US, 2003, pp. 63–79.

[17] R. L. Owen, “Uptake and transport of intestinal macromolecules and microorganisms by M cells in Peyer’s patches-a personal and historical perspective.,” *Semin. Immunol.*, vol. 11, no. 3, pp. 157–63, Jul. 1999.

[18] S. Kerneis and E. Pringault, “Plasticity of the gastrointestinal epithelium: the M cell paradigm and opportunism of pathogenic microorganisms.,” *Semin. Immunol.*, vol. 11, no. 3, pp. 205–215, Jun. 1999.

[19] M. A. Clark, M. A. Jepson, and B. H. Hirst, “Exploiting M cells for drug and vaccine delivery.,” *Adv. Drug Deliv. Rev.*, vol. 50, no. 1–2, pp. 81–106, Aug. 2001.

[20] F. Antunes, F. Andrade, D. Ferreira, H. M. Nielsen, and B. Sarmento, “Models to predict intestinal absorption of therapeutic peptides and proteins.,” *Curr. Drug Metab.*, vol. 14, no. 1, pp. 4–20, Jan. 2013.

[21] Y. Yun, Y. W. Cho, and K. Park, “Nanoparticles for oral delivery: targeted nanoparticles with peptidic ligands for oral protein delivery.,” *Adv. Drug Deliv. Rev.*, vol. 65, no. 6, pp. 822–32, Jul. 2013.

[22] P. Shah, V. Jogani, T. Bagchi, and A. Misra, “Role of Caco-2 cell monolayers in prediction of intestinal drug absorption.,” *Biotechnol. Prog.*, vol. 22, no. 1, pp. 186–98, 2006.

[23] A. T. Florence, “Issues in oral nanoparticle drug carrier uptake and targeting.,” *J. Drug Target.*, vol. 12, no. 2, pp. 65–70, Feb. 2004.

[24] J. Lee, M. J. Cuddihy, and N. a Kotov, “Three-dimensional cell culture matrices: State of the art.,” *Tissue Eng. Part B. Rev.*, vol. 14, no. 1, pp. 61–86, Mar. 2008.

[25] K. Kim, K. Ohashi, R. Utoh, K. Kano, and T. Okano, “Preserved liver-specific functions of hepatocytes in 3D co-culture with endothelial cell sheets.,” *Biomaterials*, vol. 33, no. 5, pp. 1406–13, Feb. 2012.

[26] K. G. Battiston, J. W. C. Cheung, D. Jain, and J. P. Santerre, “Biomaterials in co-culture systems: towards optimizing tissue integration and cell signaling within scaffolds.,” *Biomaterials*, vol. 35, no. 15, pp. 4465–76, May 2014.

[27] D. Williams, “Chapter 9: Biocompatibility.,” in *Tissue Enginerring*, Elsevier, 2008, pp. 255–278.

[28] S. Breslin and L. O’Driscoll, “Three-dimensional cell culture: the missing link in drug discovery.,” *Drug Discov. Today*, vol. 18, no. 5–6, pp. 240–9, Mar. 2013.

[29] M. Rimann and U. Graf-Hausner, “Synthetic 3D multicellular systems for drug development.,” *Curr. Opin. Biotechnol.*, vol. 23, no. 5, pp. 803–9, Oct. 2012.

[30] S. F. Badylak, “The extracellular matrix as a scaffold for tissue reconstruction.,” vol. 13, no. 02, pp. 377–383, 2002.

[31] S. F. Badylak, “The extracellular matrix as a biologic scaffold material.,” *Biomaterials*, vol. 28, no. 25, pp. 3587–93, Sep. 2007.

[32] K. B. Fonseca, P. L. Granja, and C. C. Barrias, “Engineering proteolytically-degradable artificial extracellular matrices.,” *Prog. Polym. Sci.*, Jul. 2014.

[33] S. Badylak, T. Gilbert, and J. Myers-irvin, “Chapter 5: The extracellular matrix as a biologic scaffold for tissue engineering.,” in *Tissue Enginerring*, Elsevier, 2008, pp. 121–143.

[34] M. W. Tibbitt and K. S. Anseth, “Hydrogels as extracellular matrix mimics for 3D cell culture.,” *Biotechnol. Bioeng.*, vol. 103, no. 4, pp. 655–63, Jul. 2009.

[35] S. J. Bidarra, C. C. Barrias, and P. L. Granja, “Injectable alginate hydrogels for cell delivery in tissue engineering.,” *Acta Biomater.*, vol. 10, no. 4, pp. 1646–1662, Apr. 2014.

[36] A. S. Hoffman, “Hydrogels for biomedical applications.,” *Adv. Drug Deliv. Rev.*, vol. 54, no. 1, pp. 3–12, Jan. 2002.

[37] A. K. Gaharwar, N. a Peppas, and A. Khademhosseini, “Nanocomposite hydrogels for biomedical applications.,” *Biotechnol. Bioeng.*, vol. 111, no. 3, pp. 441–53, Mar. 2014.

[38] A. D. Augst, H. J. Kong, and D. J. Mooney, “Alginate hydrogels as biomaterials.,” *Macromol. Biosci.*, vol. 6, no. 8, pp. 623–33, Aug. 2006.

[39] K. I. Draget, S. Olav, and G. Skjak-Braek, “Alginates from algae.,” in *Biopolymers Online*, A. Steinbüchel, Ed. Weinheim, Germany: Wiley-VCH Verlag GmbH & Co. KGaA, 2005, pp. 1–30.

[40] K. Y. Lee and D. J. Mooney, “Alginate: properties and biomedical applications.,” *Prog. Polym. Sci.*, vol. 37, no. 1, pp. 106–126, Jan. 2012.

[41] A. Astashkina, B. Mann, and D. W. Grainger, “A critical evaluation of in vitro cell culture models for high-throughput drug screening and toxicity.,” *Pharmacol. Ther.*, vol. 134, no. 1, pp. 82–106, Apr. 2012.

[42] K.-S. Vellonen, M. Malinen, E. Mannermaa, A. Subrizi, E. Toropainen, Y.-R. Lou, H. Kidron, M. Yliperttula, and A. Urtti, “A critical assessment of in vitro tissue models for ADME and drug delivery.,” *J. Control. Release*, vol. 190, pp. 94–114, Sep. 2014.

[43] J. Yu, R. L. Carrier, J. C. March, and L. G. Griffith, “Three dimensional human small intestine models for ADME-Tox studies.,” *Drug Discov. Today*, vol. 19, no. 10, pp. 1587–94, Oct. 2014.

[44] L. Wang, S. K. Murthy, G. a Barabino, and R. L. Carrier, “Synergic effects of crypt-like topography and ECM proteins on intestinal cell behavior in collagen based membranes.,” *Biomaterials*, vol. 31, no. 29, pp. 7586–98, Oct. 2010.

[45] J. H. Sung, J. Yu, D. Luo, M. L. Shuler, and J. C. March, “Microscale 3-D hydrogel scaffold for biomimetic gastrointestinal (GI) tract model.,” *Lab Chip*, vol. 11, no. 3, pp. 389–92, Feb. 2011.

[46] J. Yu, S. Peng, D. Luo, and J. C. March, “In vitro 3D human small intestinal villous model for drug permeability determination.,” *Biotechnol. Bioeng.*, vol. 109, no. 9, pp. 2173–8, Sep. 2012.

[47] F. Leonard, E. Collnot, and C. Lehr, “A three-dimensional coculture of enterocytes, monocytes and dendritic cells to model inflamed intestinal mucosa in vitro.,” *Mol. Pharm.*, vol. 7, no. 6, pp. 2103–19, Dec. 2010.

[48] FMC BioPolymer, “Keltone HVCR.,” 2008. [Online]. Available: http://www.signetchem.com/downloads/datasheets/Fmc-biopolymer/Keltone-Hvcr-Specifications.pdf. [Accessed: 22-Feb-2014].

[49] FMC BioPolymer, “Keltone LVCR,” 2005. [Online]. Available: http://www.signetchem.com/downloads/datasheets/Fmc-biopolymer/Keltone-Lvcr-Specifications.pdf. [Accessed: 22-Feb-2014].

[50] FMC BioPolymer, “Sodium alginate.,” 2008. [Online]. Available: http://www.fmcbiopolymer.com/Portals/ISP/Content/Docs/Sodium Alginate List_08.pdf. [Accessed: 22-Feb-2014].

[51] Kelco, *Alginate products for scientific water control.*, 3th ed. 1987, pp. 1–41.

[52] C. V. Liew, L. W. Chan, A. L. Ching, and P. W. S. Heng, “Evaluation of sodium alginate as drug release modifier in matrix tablets.,” *Int. J. Pharm.*, vol. 309, no. 1–2, pp. 25–37, Feb. 2006.

[53] NovaMatrix, “PRONOVA UPLVM,” 2012. [Online]. Available: http://www.novamatrix.biz. [Accessed: 20-Jul-2015].

[54] C. Kuo and P. Ma, “Ionically crosslinked alginate hydrogels as scaffolds for tissue engineering: Part 1. Structure, gelation rate and mechanical properties.,” *Biomaterials*, vol. 22, no. 6, pp. 511–21, Mar. 2001.

[55] QGelB, “The 3D matrix for life science.,” 2010. [Online]. Available: http://www.qgelbio.com/pdf/QGel_Technology_Brochure.pdf. [Accessed: 11-Jun-2014].

[56] A. W. Chan and R. J. Neufeld, “Modeling the controllable pH-responsive swelling and pore size of networked alginate based biomaterials.,” *Biomaterials*, vol. 30, no. 30, pp. 6119–29, Oct. 2009.

[57] J. a. Rowley, G. Madlambayan, and D. J. Mooney, “Alginate hydrogels as synthetic extracellular matrix materials.,” *Biomaterials*, vol. 20, no. 1, pp. 45–53, Jan. 1999.

[58] S. N. Pawar and K. J. Edgar, “Alginate derivatization: a review of chemistry, properties and applications.,” *Biomaterials*, vol. 33, no. 11, pp. 3279–305, Apr. 2012.

[59] F. R. Maia, K. B. Fonseca, G. Rodrigues, P. L. Granja, and C. C. Barrias, “Matrix-driven formation of mesenchymal stem cell-extracellular matrix microtissues on soft alginate hydrogels.,” *Acta Biomater.*, vol. 10, no. 7, pp. 3197–208, Jul. 2014.

[60] F. R. Maia, A. H. Lourenço, P. L. Granja, R. M. Gonçalves, and C. C. Barrias, “Effect of cell density on mesenchymal stem cells aggregation in RGD-alginate 3D matrices under osteoinductive conditions.,” *Macromol. Biosci.*, pp. 1–13, Feb. 2014.

[61] C. Pereira, F. Araújo, C. C. Barrias, P. L. Granja, and B. Sarmento, “Dissecting stromal-epithelial interactions in a 3D in vitro cellularized intestinal model for permeability studies.,” *Biomaterials*, vol. 56, pp. 36–45, Jul. 2015.

[62] B. Sarmento, A. Ribeiro, F. Veiga, and D. Ferreira, “Development and validation of a rapid reversed-phase HPLC method for the determination of insulin from nanoparticulate systems.,” *Biomed. Chromatogr.*, vol. 20, no. 9, pp. 898–903, Sep. 2006.

[63] B. Lee, B. Li, and S. a Guelcher, “Gel microstructure regulates proliferation and differentiation of MC3T3-E1 cells encapsulated in alginate beads.,” *Acta Biomater.*, vol. 8, no. 5, pp. 1693–702, May 2012.

[64] L. Wang, R. M. Shelton, P. R. Cooper, M. Lawson, J. T. Triffitt, and J. E. Barralet, “Evaluation of sodium alginate for bone marrow cell tissue engineering.,” *Biomaterials*, vol. 24, no. 20, pp. 3475–3481, Sep. 2003.

[65] N. E. Simpson, C. L. Stabler, C. P. Simpson, A. Sambanis, and I. Constantinidis, “The role of the CaCl2–guluronic acid interaction on alginate encapsulated βTC3 cells.,” *Biomaterials*, vol. 25, no. 13, pp. 2603–2610, Jun. 2004.

[66] J. Chen, R. Zhou, L. Li, B. Li, X. Zhang, and J. Su, “Mechanical, rheological and release behaviors of a poloxamer 407/ poloxamer 188/carbopol 940 thermosensitive composite hydrogel.,” *Molecules*, vol. 18, no. 10, pp. 12415–25, Jan. 2013.

[67] M. J. Ramazani-Harandi, M. J. Zohuriaan-Mehr, A. a. Yousefi, A. Ershad-Langroudi, and K. Kabiri, “Rheological determination of the swollen gel strength of superabsorbent polymer hydrogels.,” *Polym. Test.*, vol. 25, no. 4, pp. 470–474, Jun. 2006.

[68] “Swelling measurements of crosslinked polymers .,” *Cambridge Polymer Group*. [Online]. Available: http://www.campoly.com/files/3013/5216/6056/005.pdf. [Accessed: 10-Sep-2015].

[69] O. Jeon, S. J. Song, K.-J. Lee, M. H. Park, S.-H. Lee, S. K. Hahn, S. Kim, and B.-S. Kim, “Mechanical properties and degradation behaviors of hyaluronic acid hydrogels cross-linked at various cross-linking densities,” *Carbohydr. Polym.*, vol. 70, no. 3, pp. 251–257, Oct. 2007.

[70] R. G. Wells, “The role of matrix stiffness in regulating cell behavior.,” *Hepatology*, vol. 47, no. 4, pp. 1394–400, Apr. 2008.

[71] K. Bott, Z. Upton, K. Schrobback, M. Ehrbar, J. a Hubbell, M. P. Lutolf, and S. C. Rizzi, “The effect of matrix characteristics on fibroblast proliferation in 3D gels.,” *Biomaterials*, vol. 31, no. 32, pp. 8454–64, Nov. 2010.

[72] H. Kong, M. Smith, and D. Mooney, “Designing alginate hydrogels to maintain viability of immobilized cells.,” *Biomaterials*, vol. 24, no. 22, pp. 4023–4029, Oct. 2003.

[73] D. W. Powell, P. a Adegboyega, J. F. Di Mari, and R. C. Mifflin, “Epithelial cells and their neighbors I. Role of intestinal myofibroblasts in development, repair, and cancer.,” *Am. J. Physiol. Gastrointest. Liver Physiol.*, vol. 289, no. 1, pp. G2–7, Jul. 2005.

[74] S.-F. Lan and B. Starly, “Alginate based 3D hydrogels as an in vitro co-culture model platform for the toxicity screening of new chemical entities.,” *Toxicol. Appl. Pharmacol.*, vol. 256, no. 1, pp. 62–72, Oct. 2011.

[75] S. Talukdar, Q. T. Nguyen, A. C. Chen, R. L. Sah, and S. C. Kundu, “Effect of initial cell seeding density on 3D-engineered silk fibroin scaffolds for articular cartilage tissue engineering.,” *Biomaterials*, vol. 32, no. 34, pp. 8927–37, Dec. 2011.

[76] K. M. Hakkinen, J. S. Harunaga, A. D. Doyle, and K. M. Yamada, “Direct comparisons of the morphology, migration, cell adhesions, and actin cytoskeleton of fibroblasts in four different three-dimensional extracellular matrices.,” *Tissue Eng. Part A*, vol. 17, no. 5–6, pp. 713–24, Mar. 2011.

[77] C. Branco da Cunha, D. D. Klumpers, W. a Li, S. T. Koshy, J. C. Weaver, O. Chaudhuri, P. L. Granja, and D. J. Mooney, “Influence of the stiffness of three-dimensional alginate/collagen-I interpenetrating networks on fibroblast biology.,” *Biomaterials*, vol. 35, no. 32, pp. 8927–36, Oct. 2014.

[78] R. J. Pelham and Y. l Wang, “Cell locomotion and focal adhesions are regulated by substrate flexibility.,” *Proc. Natl. Acad. Sci. U. S. A.*, vol. 94, no. 25, pp. 13661–5, Dec. 1997.

[79] J. Solon, I. Levental, K. Sengupta, P. C. Georges, and P. a Janmey, “Fibroblast adaptation and stiffness matching to soft elastic substrates.,” *Biophys. J.*, vol. 93, no. 12, pp. 4453–61, Dec. 2007.

[80] J. A. Green and K. M. Yamada, “Three-Dimensional microenviroments modulate fibroblast signaling responses.,” *Adv Drug Deliv Rev*, vol. 59, no. 13, pp. 1293–1298, 2008.

[81] R. O. Hynes, “Integrins : bidirectional , allosteric signaling machines in their roles as major adhesion receptors , integrins.,” vol. 110, no. Table 1, pp. 673–687, 2002.

[82] E. E. Robinson, R. A. Foty, and S. A. Corbett, “Fibronectin matrix assembly regulates alpha5beta1-mediated cell cohesion.,” *Mol. Biol. Cell*, vol. 15, no. 3, pp. 973–81, Mar. 2004.

[83] J. R. Couchman, M. Höök, D. A. Rees, and R. Timpl, “Adhesion, growth, and matrix production by fibroblasts on laminin substrates,” *J. Cell Biol.*, vol. 96, no. 1, pp. 177–183, Jan. 1983.

[84] E. A. Voger and R. W. Bussian, “Short-term cell-attachment rates: a surface-sensitive test of cell-substrate compatibility.,” *J. Biomed. Mater. Res.*, vol. 21, no. 10, pp. 1197–211, Oct. 1987.

[85] C. Hilgendorf, H. Spahn-Langguth, C. G. Regårdh, E. Lipka, G. L. Amidon, and P. Langguth, “Caco-2 versus Caco-2/HT29-MTX co-cultured cell lines: permeabilities via diffusion, inside- and outside-directed carrier-mediated transport.,” *J. Pharm. Sci.*, vol. 89, no. 1, pp. 63–75, Jan. 2000.

[86] Daugherty and Mrsny, “Transcellular uptake mechanisms of the intestinal epithelial barrier Part one.,” *Pharm. Sci. Technolo. Today*, vol. 4, no. 2, pp. 144–151, Apr. 1999.

[87] P. Artursson, K. Palm, and K. Luthman, “Caco-2 monolayers in experimental and theoretical predictions of drug transport.,” *Adv. Drug Deliv. Rev.*, vol. 64, pp. 280–289, Dec. 2012.

[88] L. Yin, J. Ding, L. Fei, M. He, F. Cui, C. Tang, and C. Yin, “Beneficial properties for insulin absorption using superporous hydrogel containing interpenetrating polymer network as oral delivery vehicles.,” *Int. J. Pharm.*, vol. 350, no. 1–2, pp. 220–229, Feb. 2008.

[89] L. Yin, J. Ding, C. He, L. Cui, C. Tang, and C. Yin, “Drug permeability and mucoadhesion properties of thiolated trimethyl chitosan nanoparticles in oral insulin delivery.,” *Biomaterials*, vol. 30, no. 29, pp. 5691–5700, Oct. 2009.

[90] C. B. Woitiski, B. Sarmento, R. A. Carvalho, R. J. Neufeld, and F. Veiga, “Facilitated nanoscale delivery of insulin across intestinal membrane models.,” *Int. J. Pharm.*, vol. 412, no. 1–2, pp. 123–131, Jun. 2011.

[91] M. Leonard, E. Creed, D. Brayden, and A. W. Baird, “Evaluation of the Caco-2 monolayer as a model epithelium for iontophoretic transport.,” *Pharm. Res.*, vol. 17, no. 10, pp. 1181–1188, Oct. 2000.

[92] D. A. Carr and N. A. Peppas, “Assessment of poly(methacrylic acid-co-N-vinyl pyrrolidone) as a carrier for the oral delivery of therapeutic proteins using Caco-2 and HT29-MTX cell lines.,” *J. Biomed. Mater. Res. A*, vol. 92, no. 2, pp. 504–12, Feb. 2010.